Nonlinear shear and extensional flow dynamics of wormlike surfactant solutions

B. Yesilata [a,b,*], C. Clasen [a,c], G.H. McKinley [a]

[a] *Department of Mechanical Engineering, Hatsopoulos Microfluid Laboratory, M.I.T., Cambridge, MA 02139, USA*
[b] *Department of Mechanical Engineering, Harran University, Osmanbey Campus, Sanliurfa 63300, Turkey*
[c] *Institute of Technical and Macromolecular Chemistry, University of Hamburg, 22041 Hamburg, Germany*

Abstract

Nonlinear shear and extensional flow dynamics of a wormlike micellar solution based on erucyl bis(2-hydroxyethyl) methyl ammonium chloride (EHAC) are reported here. The influences of surfactant (EHAC) and salt (NH_4Cl) concentrations on the linear viscoelastic parameters are determined using small amplitude oscillatory shear experiments. The steady and time-dependent shear rheology is determined in a double gap Couette cell, and transient extensional flow measurements are performed in a capillary breakup extensional rheometer (CABER). In the nonlinear shear flow experiments, the micellar fluid samples show strong hysteretic behavior upon increasing and decreasing the imposed shear stress due to the development of shear-banding instabilities. The non-monotone flow curves of stress versus shear rate can be successfully modeled in a macroscopic sense by using the single-mode Giesekus constitutive equation. The temporal evolution of the flow structure of the surfactant solutions in the Couette flow geometry is analyzed by instantaneous shear rate measurements for various values of controlled shear stress, along with FFT analysis. The results indicate that the steady flow bifurcates to a global time-dependent state as soon as the shear-banding/hysteresis regime is reached. Increasing the salt–surfactant ratio or the temperature is found to stabilize the flow, and corresponds to decreasing values of anisotropy factor in the Giesekus model. Finally, we have investigated the dynamics of capillary breakup of the micellar fluid samples in uniaxial extensional flow. The filament thinning behavior of the micellar fluid samples is also accurately predicted by the Giesekus constitutive equation. Indeed quantitative agreement between the experimental and numerical results can be obtained providing that the relaxation time of the wormlike micellar solutions in extensional flows is a factor of three lower than in shear flows.
© 2005 Elsevier B.V. All rights reserved.

Keywords: Nonlinear; Wormlike micelles; Extensional flow; Capillary breakup extensional rheometry; Shear banding; Hysteresis

1. Introduction

Surfactant molecules consist of a hydrophilic head group and a hydrophobic tail and under certain conditions they can spontaneously self-assemble into long, flexible wormlike micelles in aqueous solutions. The structure and rheology of these micelles are extremely sensitive to surfactant and counterion concentration as well as to temperature because the individual micelles are constantly being destroyed and recreated through Brownian fluctuations. Wormlike micellar systems are therefore widely used in industry as viscosity modifiers and enhancers [1,2]. They also offer potential as drag-reduction additives in district heating systems [3]. Recently, wormlike micellar systems have been suc-cessfully used in separation of DNA fragments [4] and in forming templates for nanostructures [5]. They are also used as rheology and flow control agents in petroleum transport systems [6]. The main advantage of these liquids for enhanced oil recovery is their ability to undergo dramatic structural changes upon contacting hydrocarbons, leading to an important drop in "viscosity" (after completing its fracturing task, this liquid can be easily removed from the parts of the fracture contacting with hydrocarbon). The fracture cleanup is therefore greatly improved especially in production zones. The ability to easily formulate the fluid outdoors makes these liquids very attractive and commercially successful for oil extraction applications [7–10].

A cationic surfactant, erucyl bis(2-hydroxyethyl) methyl amomonium chloride (EHAC), has very recently been used in several studies with different counterions (EHAC/NaSal/Water, EHAC/NaCl/Water and EHAC/NaTos/Water [11–13]; EHAC/2-propanol/KCl/Water [14] and EHAC/KCl/Water [15]). Ragha-

* Corresponding author. Tel.: +90 536 7360900; fax: +90 414 3440031.
E-mail address: byesilata@yahoo.com (B. Yesilata).

van and Kaler [11] have reported that EHAC-based solutions can form an entangled network of extremely long wormlike micellar chains and become highly viscoelastic or gel-like with increasing salt concentration. The ability of these surfactant systems to form long, polymerlike structures, but with the additional possibility of breakage and reformation at much lower scission energy, leads to the terminology of "living" or "equilibrium" polymers (for recent reviews on the rheology of wormlike micelles see Refs. [16–18]). EHAC solutions show robust viscoelastic behavior even at high temperatures [11,12] in comparison to other viscoelastic surfactant systems, which is important in oilfield applications.

The linear viscoelastic rheological properties of these viscoelastic wormlike micelles in brine solutions can usually be characterized, at least at low frequencies, with a single relaxation time λ and they are therefore well described by a simple Maxwell model. This narrowing of the viscoelastic spectrum is observed when the micellar breaking time λ_{br} is short compared to the diffusion or reptation timescale λ_{rep} of the whole micelle [19]. Deviations from this monoexponential relaxation behavior are observed at high frequencies due to Rouse-like behavior of the micellar segments [20–22].

The nonlinear steady shear rheology of wormlike micelles shows a much more complex behavior as indicated schematically in Fig. 1. The dimensionless shear stress ($\tau^* = \tau_{xy}/G_0$) is plotted as a function of dimensionless shear rate ($\gamma^* = \dot{\gamma}_{xy}\lambda$). The zero shear rate viscosity is given by $\eta_0 = G_0\lambda$. The stress first rises with a slope of unity and then deviates at a shear rate of γ_1^*. The stress falls with increasing shear rate after passing through a maximum stress τ_{max}^* at a shear rate γ_M^*. This maximum has been attributed by Cates and co-workers (within the scope of reptation theory) to be the maximum stress that a reptating micellar tube segment can sustain [19,23,24]. An increasing destruction rate of the tube segments due to retraction of the wormlike micelles with further increases in the shear rate results in a falling stress at shear rates $\gamma^* > \gamma_M^*$. However, the decreasing shear stress region cannot persist to infinite shear rates, and eventually an
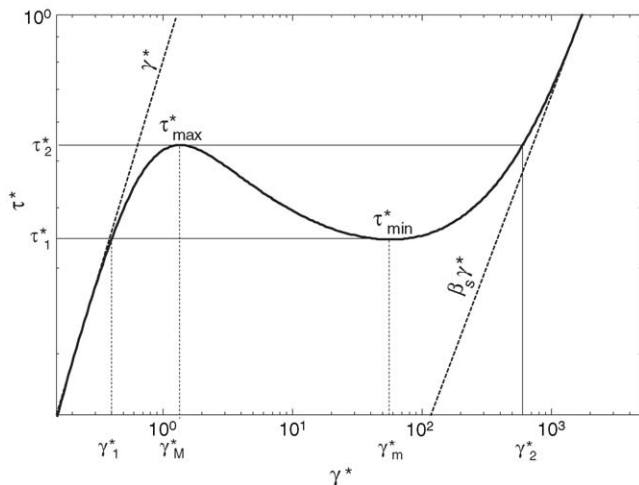
upturn in the shear stress curve is observed due to an increasing solvent contribution to the stress in the fluid sample until the stress τ_{max}^* is reached again at a shear rate γ_2^*. The separation of these two linear regions depends on the solvent viscosity ratio $\beta_s = \eta_s/\eta_0$.

Cates and co-workers [19,23,24] also developed a constitutive equation for micellar solutions based on the reptation model for steady flows with a stress tensor τ given by:

$$\tau = \frac{15}{4}G_0\left(\mathbf{W} - \frac{1}{3}\mathbf{I}\right) \tag{1}$$

where $\mathbf{W}$ is the second moment of the orientational distribution function [24]. Although this equation is able to predict the maximum behavior of the stress, it fails to capture the subsequent upturn of the stress from the solvent and disentangled chain segments. However, the nonlinear differential constitutive equation proposed by Giesekus [25,26], originally developed from a network theory for entangled polymer systems, has proven to give a very good description of the first stress maximum as well as the upturn at high shear rates [27,28]. The Giesekus model for a single relaxation mode can be written as:

$$\left(\mathbf{I} + \alpha\frac{\lambda}{\eta_p}\tau_p\right) \cdot \tau_p + \lambda\tau_{p(1)} = \eta_p\dot{\gamma}$$
$$\tau_s = \eta_s\dot{\gamma} \tag{2}$$

The symbol $\tau_{p(1)}$ denotes the upper convected derivative of the stress tensor and $\dot{\gamma}$ the rate of strain tensor and τ is the total stress given by $\tau = \tau_p + \tau_s$. Although the single-mode Giesekus model is a semi-empirical constitutive equation (incorporating an adjustable anisotropy factor α), its "spectacularly successful description of semidilute wormlike micelles" [1] in nonlinear shear flow makes it a very useful tool in the description of the reported hysteresis behavior of the flow curves in the present paper. Recent experiments using another gel-like surfactant system also show excellent agreement with the predictions of the Giesekus model in transient shear flow [29].

If an applied shear rate lies in the regime $\gamma_M^* < \gamma^* < \gamma_m^*$, a homogenous flow can no longer be stable and the system evolves towards a new stationary state, in which the system forms one or more "shear-bands" [30–32]. Thus, a steady shear flow can only be supported by separate regions of fluid flowing at the high γ_2^* and low γ_1^* shear rate limits of the stress plateau region indicated by the dotted line in Fig. 1. According to this picture, there is no constraint on the number of band configurations, and a set of multiple stationary flow states is possible in a shear rate controlled situation. Still, the stress in this plateau regime is uniform throughout the shear-bands and at the interface(s) between bands. In order to select the number and location of these bands a higher order theory is required, which incorporates spatial fluctuations across the gap in the number of density or concentrations of the micellar species [31–33].

An even more complex rheological response is expected for the case of a shear induced structure (SIS) formation (such as gelation [34] or liquid crystalline phases [35,36]), which can occur in a micellar solution. Such dynamical transitions have been theoretically described by Olmsted and co-workers [33,37]

Fig. 1. A representative nonmonotonic dimensionless stress-deformation rate relation in shear flow of a wormlike micellar solution.

and also monitored experimentally by Fuller and co-workers [38,39].

In the following report we will focus on a relatively new surfactant system with a pronounced viscosity enhancement (several orders of magnitude higher than that for comparable systems) and with unusually rich equilibrium phase behavior. The corresponding surfactants exhibit both shear-induced phase separation (SIPS) and nonzero dichroism signal under shear [13]. In these systems, a slowly increasing shear rate ramp is expected to result in a stable flow up to the maximum stress τ^*_{max} in the plateau level as indicated by the dashed line in Fig. 1 [24,40] and this typical stress behavior of an up-ramp shear rate profile has been reported by several authors [41,42]. However, beyond the critical shear rate, the stress level corresponding to the plateau region can lie between the maximum stress τ^*_{max} and the stress τ^*_{min} at the local minimum in Fig. 1. Fischer and co-workers [38,43,44] demonstrated that the dynamics of the inhomogeneous shear-band layers coexisting at such stress levels could also lead to periodic oscillatory fluctuations of the stress around this average plateau level. Very recent studies [39,45–48] have also confirmed that many shear-banding systems display periodic oscillations and time-chaotic fluctuations in their bulk rheology, rheo-optics or velocimetry. It may thus be anticipated that the final stationary stress state of the flow in the plateau regime is strongly history-dependent and a hysteresis between the measured macroscopic behavior upon increasing and decreasing the shear rate is expected [49,50]. However, there have been no detailed experiments reported of such phenomena. We will examine this hysteretic behavior under controlled stress conditions, for EHAC-based wormlike micellar fluid samples.

The extensional flow behavior of viscoelastic wormlike micelles has received far less attention than studies of the shear rheology to date. However, recent reports on flow phenomena occurring in wormlike micellar solutions, such as rising bubbles in micellar solutions [51], falling spheres and flow past spheres [52,53] or filament rupture [54,55] of wormlike micellar solutions have taken into account not only the shear flow properties, but also the steady and transient elongational viscoelastic properties of the solution.

The first investigations of the apparent extensional viscosity of wormlike micellar solutions were conducted by Prudhomme and Warr [56], Walker et al. [57], Fischer et al. [58] and Lu et al. [59], using the opposed jet device. They reported a general thickening of wormlike micellar solutions with imposed extension rate in contrast to the reported shear thinning behavior. An observed drop of the extensional viscosity at high extension rates was explained by Chen and Warr [60] by micellar scission at high rates and supported with measurements of the radius of gyration in the extensional flow field of the opposed jet device. However, severe problems in the quantitative correlation of the material functions determined with the opposed jet device [61] have led to other methods for studying extensional flows. Kato et al. [62] used rheo-optical studies in a four roller mill, and Muller et al. [63] investigated the flow through porous media to measure steady elongational viscosities. For robust determination of the transient elongational viscosity, wormlike micellar solutions were investigated recently with a capillary breakup rheometer

by Anderson et al. [64], using the EHAC system reported on in the current paper, and with a filament stretching rheometer by Rothstein [65], who was able to calculate a scission energy for wormlike micelles in strong extensional flows, supporting the hypothesis of Chen and Warr [60] for the drop in the extensional viscosity at high rates.

In the present study, we examine the hysteretic behavior of wormlike micellar fluid solutions in nonlinear shear experiments upon increasing and decreasing the deformation rate under controlled shear stress conditions for different temperatures and salt concentrations. We compare these results with the theoretical predictions of the single-mode Giesekus model using parameters that are independently determined from linear viscoelastic data obtained using small amplitude oscillatory flow experiments. The Giesekus equation is then used to predict the behavior of wormlike micellar solutions in a uniaxial extensional flow field. These theoretical results are then compared to experimental measurements of the transient extensional response of wormlike micellar solutions determined using the capillary breakup extensional rheometer (CABER).

2. Experimental

2.1. Apparatus

The oscillatory and steady shear flow measurements were performed with an AR 2000 stress controlled rheometer (T.A. Instruments, Newcastle DE, USA) in a double gap concentric cylinder fixture (rotor outer radius: 21.96 mm, rotor inner radius: 20.38 mm, gap: 0.5 mm, approximate sample volume: 6.48 ml and cylinder immersed height: 59.5 mm). Extensional flow measurements were conducted in a capillary breakup extensional rheometer developed in collaboration with the Cambridge Polymer Group (Cambridge, MA, USA). The device holds a fluid sample between circular plates (with radius of 3 mm, initial plate separation of 2.2 mm). An axial step strain is imposed by separating the plates rapidly within 50 ms to a final separation of 6.6 mm. The midpoint diameter of the fluid filament is monitored using a laser micrometer with a calibrated minimum resolution of 20 μm. The global evolution of the column profile is also recorded with a standard CCD camera. More detailed description about the CABER device is given elsewhere [66–68].

2.2. Fluid samples

The surfactant solution, a mixture of erucyl bis(2-hydroxyethyl) methyl ammonium chloride and iso-propanol (25 wt%), is obtained from Schlumberger Cambridge Research. The fluid samples to be studied were diluted with an appropriate amount of brine solution (ammonium chloride in deionized water) and stirred to homogeneity for 72 h. The samples are then kept at rest for a time-period of 7 days prior to the measurements.

Two sets of fluid samples were prepared to investigate the effects of EHAC concentration (C_{surf}) and the molar concentration ratio of NH_4Cl/EHAC ($C^* = C_{salt}/C_{surf}$). For the first set of six samples the EHAC concentration (54 mM or 2.25 wt%) was held constant while NH_4Cl concentrations were varied from

143 mM (0.75 wt%) to 858 mM (4.5 wt%) with increments of 143 mM (0.75 wt%). For the second set of five samples, the molar concentration ratio of NH₄Cl/EHAC was kept constant ($C^* = 10.6$) and the surfactant concentration was varied from 18 mM (0.75 wt%) to 90 mM (3.75 wt%) with an increment of 18 mM (0.75 wt%).

3. Results and discussion

3.1. Linear viscoelastic behavior of micellar solutions

It is now well known that viscoelastic surfactant solutions can behave, under certain conditions, like an ideal Maxwell material with a single characteristic relaxation time, λ, for the whole system. However, the linear rheological properties of wormlike micellar solutions depend on the ratio of breaking and reptation times, denoted

$$\zeta = \frac{\lambda_{br}}{\lambda_{rep}} \tag{3}$$

where the weak micellar structures break and recombine on an individual timescale denoted λ_{br}. According to Cates and co-workers [19,20,23,69] a single exponential relaxation is only observed if $\lambda_{br} \ll \lambda_{rep}$. In this case the breaking time (the aver-age lifetime) of the micelles is much smaller than the reptation time (the diffusion time). Numerous breaking and re-formation processes occur within the time scale of the overall relaxation and consequently average out the relaxation process leading to a pure, monoexponential stress decay. On the basis of reptation theory [70], Cates [23] developed an expression for this single relaxation time depending on the breakup and reptation time:

$$\lambda = (\lambda_{br}\lambda_{rep})^{0.5}. \tag{4}$$

The linear viscoelastic (LVE) behavior of complex fluids can be described in terms of the complex relaxation modulus G^*

$$G^*(\omega) = G'(\omega) + iG''(\omega) \tag{5}$$

where the storage modulus, $G'(\omega)$, and the loss modulus, $G''(\omega)$, are expressed for an ideal Maxwell model with a single relaxation time by

$$G'(\omega) = G_0 \frac{\omega^2\lambda^2}{1 + \omega^2\lambda^2} \tag{6}$$

$$G''(\omega) = G_0 \frac{\omega\lambda}{1 + \omega^2\lambda^2}. \tag{7}$$

In Fig. 2, we show the remarkable agreement of the experimental data ($T = 25\,°C$) at low and medium frequencies with
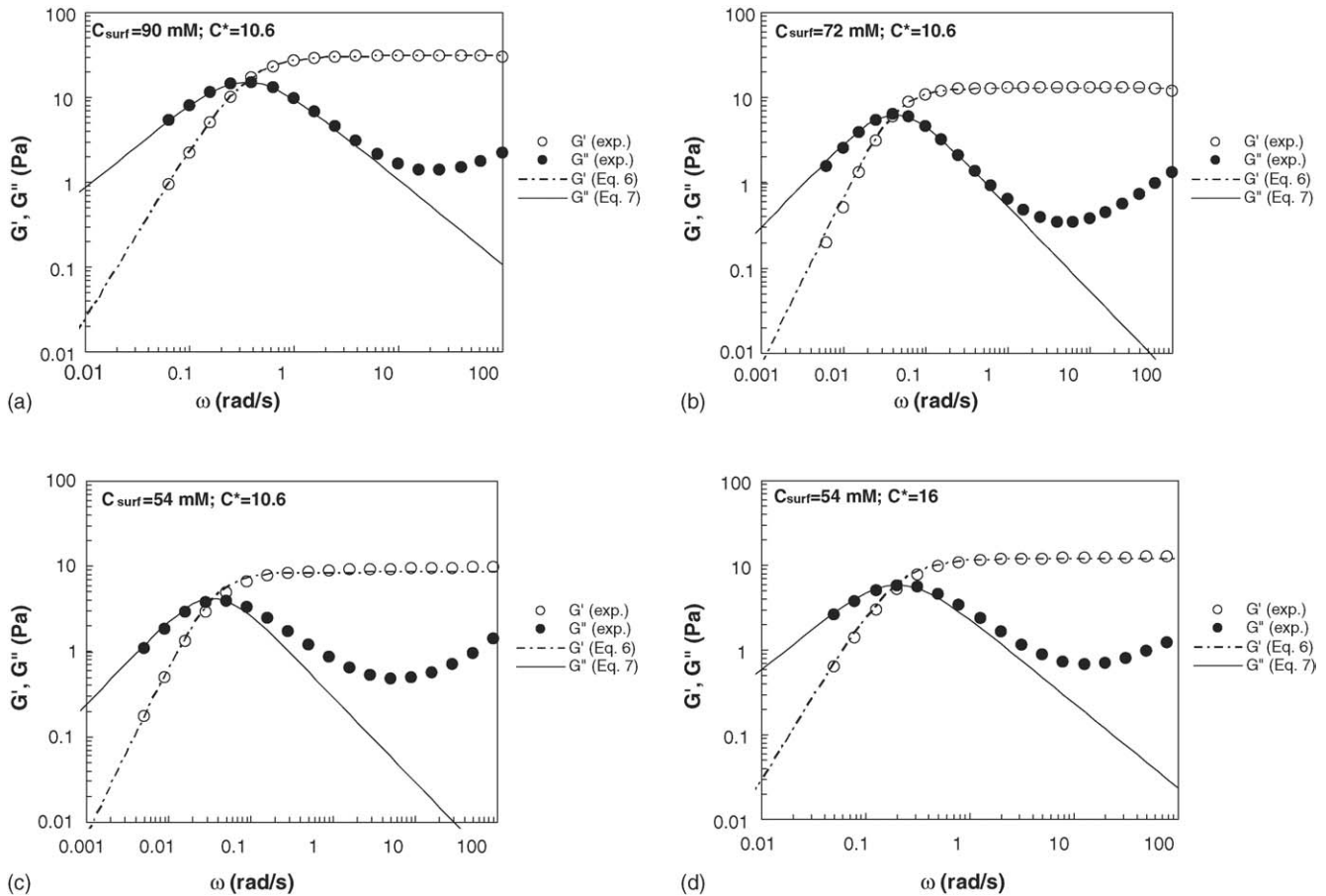

Fig. 2. The storage moduli, $G'(\omega)$, and the loss moduli, $G''(\omega)$, determined in a frequency range of 0.01–100 rad/s with a constant shear strain of 10% for the EHAC solutions of: (a) $C_{surf} = 90$ mM; $C^* = 10.6$, (b) $C_{surf} = 72$ mM; $C^* = 10.6$, (c) $C_{surf} = 54$ mM; $C^* = 10.6$ and (d) $C_{surf} = 54$ mM; $C^* = 16$ (experiments were performed at $T = 25\,°C$).

this single relaxation time Maxwell model. The deviations from Maxwellian behavior in general start at higher frequencies for larger values of C_{surf} (for constant C^*) and larger values of C^* (for constant C_{surf}). The relaxation time λ and the plateau modulus G_0 were determined from a least squares fit of the Maxwell model (Eqs. (6) and (7)) to the measured LVE data. This was done using a Cole–Cole representation of the storage and loss moduli as shown in Fig. 3. In these plots, the loss modulus is plotted as a function of the storage modulus, and this enables a more precise determination of the relaxation behavior of samples than simple frequency sweeps [20]. Semi-circular profiles are obtained from the Maxwell model and represent the pure mono-exponential stress relaxation behavior at $T = 25\,^\circ C$. Fig. 3(a) shows the effect of the surfactant concentration (C_{surf}) on the linear viscoelastic behavior for a constant salt–surfactant concentration ratio of $C^* = 10.6$, whereas Fig. 3(b) shows the effects of varying salt concentration at a constant surfactant concentration of $C_{surf} = 54$ mM. The diameter of the semi-circular shape is a measure of G_0 and is greatly affected by variation in C_{surf}. A monotonic decrease in the diameter is obtained with lower values of C_{surf}, rapidly dropping to the lowest value of 0.45 Pa for the fluid sample with $C_{surf} = 18$ mM. We use an inset to Fig. 3(a) in order to more clearly illustrate the semi-circular shape for this sample. The fit results ($T = 25\,^\circ C$) are given in Table 1 and shown in Fig. 4.

In the absence of any solvent contribution to the stress, the zero shear viscosities of the samples are calculated by

$$\eta_0 = \eta_p = G_0\lambda. \tag{8}$$

The dashed lines in Fig. 4(a and b) are best fits from regression analysis and are shown here to qualitatively illustrate the general trend of the fitted rheological parameters with increasing C_{salt}. In both cases, increasing salt concentration results in
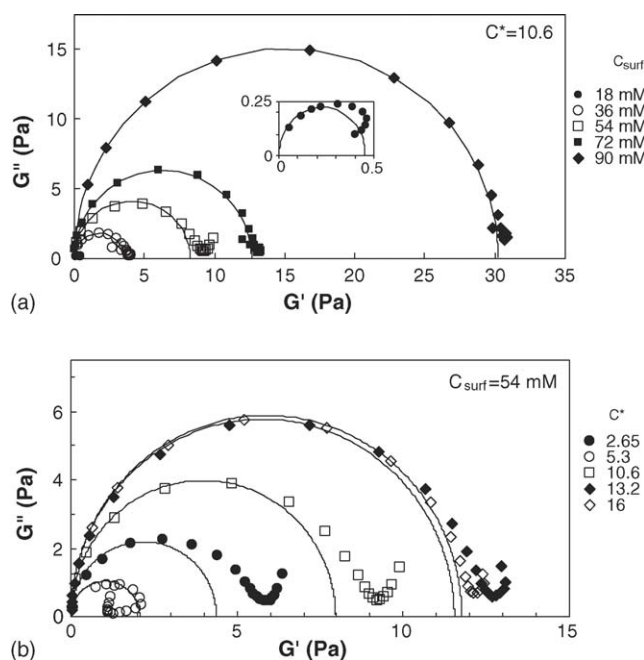

(a)

(b)

Fig. 3. Cole–Cole plots of EHAC solutions (a) for various surfactant concentrations (C_{surf}) and (b) for various salt–surfactant concentration ratios (C^*). The inset to (a) is the plot for $C_{surf} = 18$ mM. The storage modulus, $G'(\omega)$, and the loss modulus, $G''(\omega)$, are determined in a frequency range of 0.01–100 rad/s with a constant shear strain of 10% (experiments were performed at $T = 25\,^\circ C$).

a monotonic increase in G_0. The variation of plateau modulus exhibits a power law type behavior, which is expected from theoretical predictions for polymers and micellar solutions [23,69]. The corresponding relations are, respectively, $G_0 \sim (C_{salt})^{2.49}$ for $C^* = 10.6$ held constant (Fig. 4(a)) and $G_0 \sim (C_{salt})^{0.73}$ for $C_{surf} = 54$ mM held constant (Fig. 4(b)). Because the ratio of surfactant to salt (or equivalently the salinity conditions) are

Table 1
Linear viscoelastic properties of the wormlike micellar fluid samples determined from small-amplitude oscillatory shear experiments $T = 25\,^\circ C$ ($C^* = C_{salt}/C_{surf}$)

$C_{surf} = 54$ mmol/l

				E1	E2	E3
C^*	2.65	5.3	8.0	10.6	13.3	16
C_{salt} (mmol/l)	143	286	432	572	718	864
λ (s)	60.6	171	103	28.4	10.9	5
G_0 (Pa)	4.7	2.07	8.7	8.4	11.6	11.8
η_0 (Pa s)	284	355	903	238	126	59
G''_{min} (Pa)	0.474	0.096	0.246	0.48	0.599	0.681
$\lambda_{br} \times 10^2$ (s)	11.2	112.4	50.2	19.9	12.6	7.9
$\zeta \times 10^4$	0.034	0.428	0.233	0.494	1.344	2.567

$C^* = 10.6$

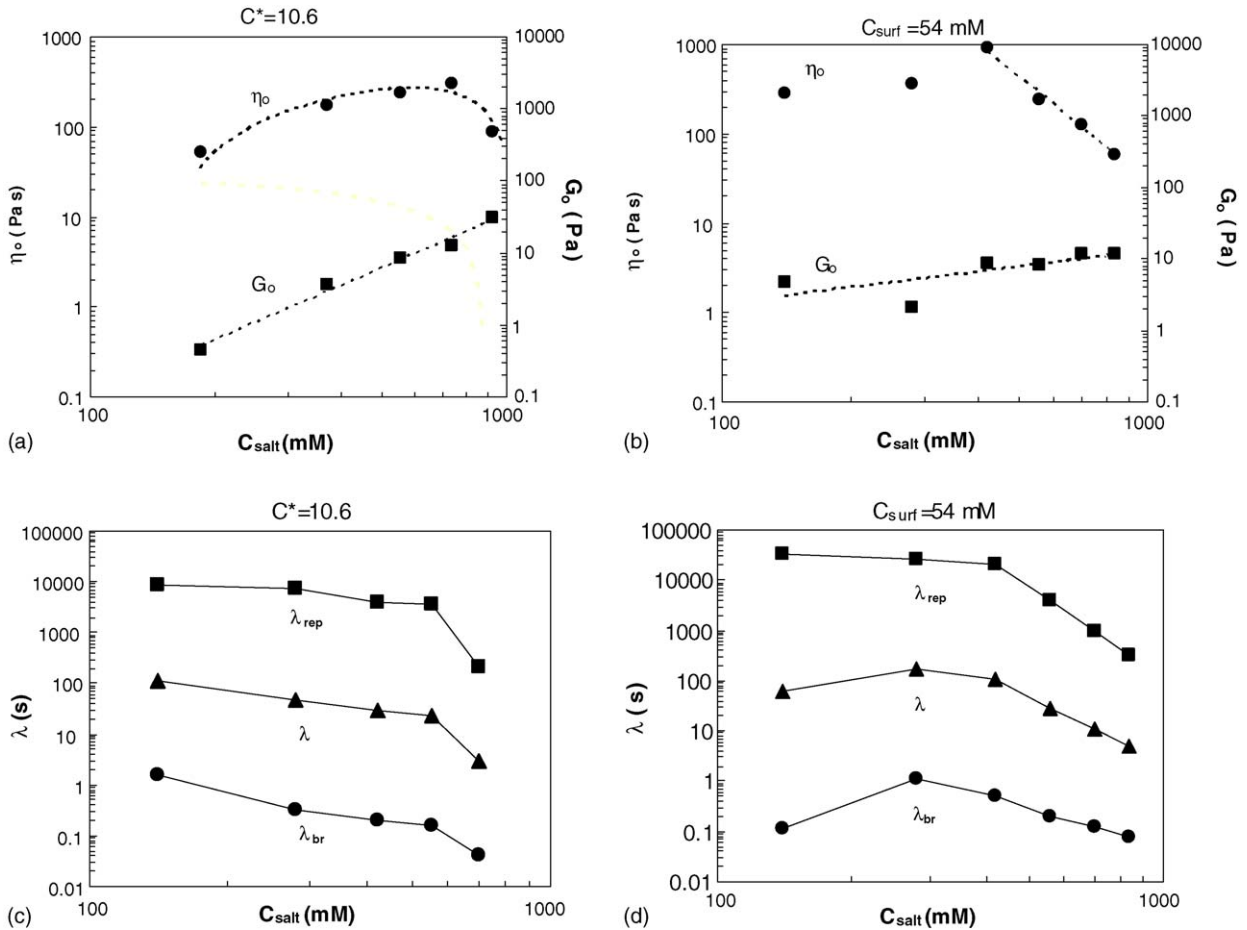|	E1				
C_{surf} (mmol/l)	18	36	54	72	90
C_{salt} (mmol/l)	191	382	572	763	954
λ (s)	115	48.7	28.4	23.7	2.9
G_0 (Pa)	0.45	3.6	8.4	12.6	30.2
η_0 (Pa s)	51.9	175	238	298	87.6
G''_{min} (Pa)	0.055	0.166	0.48	0.34	1.37
$\lambda_{br} \times 10^2$ (s)	158	31.7	19.9	15.9	3.9
$\zeta \times 10^4$	1.886	0.424	0.494	0.450	1.951

Fig. 4. Linear viscoelastic (LVE) parameters and time scales of EHAC solutions: (a) LVE parameters for various C_{surf}, (b) LVE parameters for various C^*, (c) time scales for various C_{surf} and (d) time scales for various C^* (experiments were performed at $T = 25\,°C$).

kept constant in Fig. 4(a) for a wormlike micellar solution with $C^* = 10.6$, the data actually corresponds to an increasing surfactant concentration. The observed scaling of $G_0 \sim (C_{salt})^{2.49}$ indicates that the rheological behavior of these EHAC surfactant systems in this concentration regime is in good agreement with the theoretically predicted power law exponent of 2.3 obtained from scaling theory for micellar solutions [69]. Similar scaling has also been observed for other micellar systems [71]. Raghavan and Kaler [11] have performed similar analyses for their EHAC-based solutions. Their measurements were made for a constant molar concentration ratio of $C^* = 0.5$ and for a constant surfactant concentration of $C_{surf} = 60$ mM at a temperature of $60\,°C$. Their reported values of the power–law exponents for these two cases (respectively, 2.27 and ~1) appear to be close to the ones obtained in the present study.

Fig. 4(b) shows the variation of the linear viscoelastic properties with salt concentration at a constant surfactant concentration. In this case, a ratio of $G_0 \sim (C_{salt})^{0.77}$ is observed, suggesting a rather salinity-insensitive dependence of the plateau modulus. This is in accordance with the suggestion that an increasing salt concentration does not lead to strong changes in the structural composition of the wormlike micelles at this salinity level; as a consequence, the modulus varies only weakly. However, as Safran et al. [72] have noted, the screening effect

of the salt counterions with rising concentration may lead to an alteration of the scission energy of the micelles, and therefore significant variation in the relaxation time as shown in Fig. 4(d).

At high salinities, Candau et al. [73] describe the formation of a dynamic three-dimensional network of wormlike micelles that results in a local maximum in the relaxation time and also in the resulting viscosity of the solution (see Eq. (8)). We observe a similar behavior in Fig. 4(d) for the relaxation time and in Fig. 4(b) for the viscosity. This pronounced maximum is again in agreement with the viscosity measurements of Raghavan and Kaler for an EHAC/sodium salicylate solution [11]. However, it should be noted that with the smaller Cl^- ions utilized in our study, the critical concentrations required for the maxima in the viscosity and relaxation time to be observed are nearly a decade higher. A possible explanation for this shift is that, in contrast to salicylate, the nonbinding character of the Cl^- ions limits the penetration between the head groups of the EHAC molecules that comprise the micelles, so that this screening effect requires much higher salt concentrations. The critical concentrations of the samples that correspond to maximum values of η_0 are $C_{salt} = 762$ mM (or $C_{surf} = 72$ mM) for $C^* = 10.6$ and $C_{salt} = 332$ mM (or $C^* = 8$) for $C_{surf} = 54$ mM.

We notice in Fig. 4(b) that for $C^* \geq 8$ the relationship between C_{salt} and η_0 becomes almost linear on this log–log plot with a

power law exponent, $\eta_0 \sim (C_{\text{salt}})^{-3.37}$. This value of a power law exponent is slightly lower than the power–law exponent of -5 quoted by Larson [1] and Shikata and Kotaka [74] for some gel-like surfactant systems. Clausen et al. [75] describe electron microscopy imaging studies of micelles in this region of decreasing relaxation time that demonstrate that the length of the micelles (and thus the modulus) remains fairly constant, indicating that it is indeed the screening by the increased salt concentration that accelerates the micellar reformation processes.

For clarity in our discussion of the nonlinear rheology in the following section we will focus on the three fluid samples (denoting them by E1, E2 and E3) on the power law curve of Fig. 4(b) to examine the effects of salt–surfactant ratio on nonlinear shear and extensional flow behavior. The composition of fluids E1, E2 and E3 along with other micellar fluid samples used in this work are given in Table 1.

The representation of the storage and loss moduli for the investigated solutions in the form of Cole–Cole plots (Fig. 3) shows that in all cases Maxwell-like behavior is obtained in the low-and medium-frequency regimes. However, in Fig. 3(b), significant deviations from Maxwell behavior are present at high frequencies. These deviations are expected at high frequencies because Rouse-like behavior of the individual entangled segments and an additional solvent stress are present. Consequently, there is an upturn of G'' as a function of G' as noted by Fischer and Rehage [27]. The addition of a Newtonian 'solvent-like' contribution to Eq. (7) with $\eta_s \ll G_0\lambda$, allows a better agreement at high frequency regimes while the low-frequency regime remains unaffected:

$$G''(\omega) = \eta_s\omega + G_0 \frac{\omega\lambda}{1 + \omega^2\lambda^2}. \tag{9}$$

A quantitative determination of λ_{br} is possible by fitting simulations [21] or numerical calculations [20], including the ratio ζ (from Eq. (3)) as a fitting parameter, to the experimental Cole–Cole plots. Combining Eq. (3) with Eq. (4) results in the expression

$$\lambda_{\text{br}} = \lambda\sqrt{\zeta} \tag{10}$$

and enables the calculation of λ_{br} from the relaxation time and the ratio ζ. A more accessible method to extract λ_{br} from the measured deviation of G'' from the single-mode Maxwell model was introduced by Kern and co-workers [21,22,76]. According to the method and Eq. (9), a departure from the semi-circular shape at high frequencies must be represented with a 'dip' and a 'tail' indicating Rouse-like behavior. The dip corresponds to a local minimum in the loss modulus (G''_{min}) and the ratio of G''_{min}/G_0 is directly correlated to the entanglement length and average contour length of the micelle. Thus, the critical frequency ω^* at which the minimum value of the loss modulus is obtained provides a much better measure for micellar breakup time [27]. This approach was used in this report to extract the micellar breakup timescale λ_{br} from the linear viscoelastic data. The results, as well as the value of the parameter ζ calculated from Eq. (10), are listed in Table 1. As mentioned before, the zero shear rate viscosities of the fluids E1, E2 and E3 change

in a power law fashion with salt concentration (see the log–log plot shown in Fig. 4(b)).

The values of λ_{br} and ζ further support the expected monoexponential behavior since $\zeta \ll 1$, and therefore the approximation $\lambda_{\text{br}} \ll \lambda_{\text{rep}}$ holds for almost all of the fluid samples studied. The departures from semi-circular response on a Cole–Cole plot occur at progressively higher frequencies with decreasing values of ζ as can be seen in Fig. 3. The evolutions of λ and λ_{br} with increasing salinity are quite similar as shown in Fig. 4(c and d). Both time constants monotonically decrease with increasing surfactant concentrations (C_{surf}) for a constant salt–surfactant concentration ratio of $C^* = 10.6$. However, the effect of salt concentration on λ and λ_{br} at a constant surfactant concentration is more complex. Both the relaxation and micellar breakup times exhibit a maximum at $C_{\text{salt}} = 286\,\text{mM}$ (or $C^* = 5.2$) and then rapidly decrease at higher salinity. On the other hand, the reptation time λ_{rep} remains initially unaffected by salt-variation, but then sharply decreases with increasing salt concentration. This complex dependence appears to be associated with shear-induced morphology change or phase separation of micellar fluid samples, as previously observed by Raghavan and co-workers [12,13].

3.2. Steady and transient shear flows of micellar solutions

3.2.1. Steady shear flow

The nonlinear shear rheology of the micellar solution denoted E1 (see Table 1) was determined under controlled shear stress conditions, the results are given in Fig. 5 in the form of a flow curve and the corresponding viscosity-shear rate curve. Dimensionless shear stress, shear rate and viscosity are, respectively, defined as $\tau^* = \tau/G_0$, $\gamma^* = \dot{\gamma}\lambda$, and $\eta^* = \eta/\eta_0$. The symbols correspond to discrete stresses in a continuous stepped stress ramp experiment (no rest between steps). The stress-increment of each step is equal in log-space (10 equally spaced points per decade). All experimental points displayed here were measured for an overall time of 300 s and represent the averaged signal. The top branch (hollow circles) corresponds to increasing increments in τ^* and the lower branch (hollow diamonds) to decreasing increments. Both figures show a distinct hysteresis between the increasing and decreasing stress ramp. At low stresses the fluid shows a nearly Newtonian flow behavior. However, above a critical stress $\tau^* \sim O(1)$ for an increasing stress ramp the shear rate increases rapidly and leads to a second Newtonian regime at high stresses. The huge drop (5000-fold) in the viscosity at this stress level is shown in Fig. 5(a) and is commonly associated with a yielding process, or microstructural breakdown [77]. However, the nature of this structural transition cannot simply be derived from a single steady stress experiment. As already pointed out by Cates et al. [40] it is expected for a wormlike micellar system that an increasing stress ramp experiment will show a monotone increasing shear rate, albeit with a rapid increase of the shear rate at $\tau^* > \tau^*_{\text{max}}$. However, the simple reptation theory suggests that there will be a maximum of the stress-shear rate curve as pointed out in the discussion of Fig. 1 and expected from the constitutive equation of Eq. (1). For an up-ramp stress experiment the critical stress τ_{max} for the onset of the plateau is
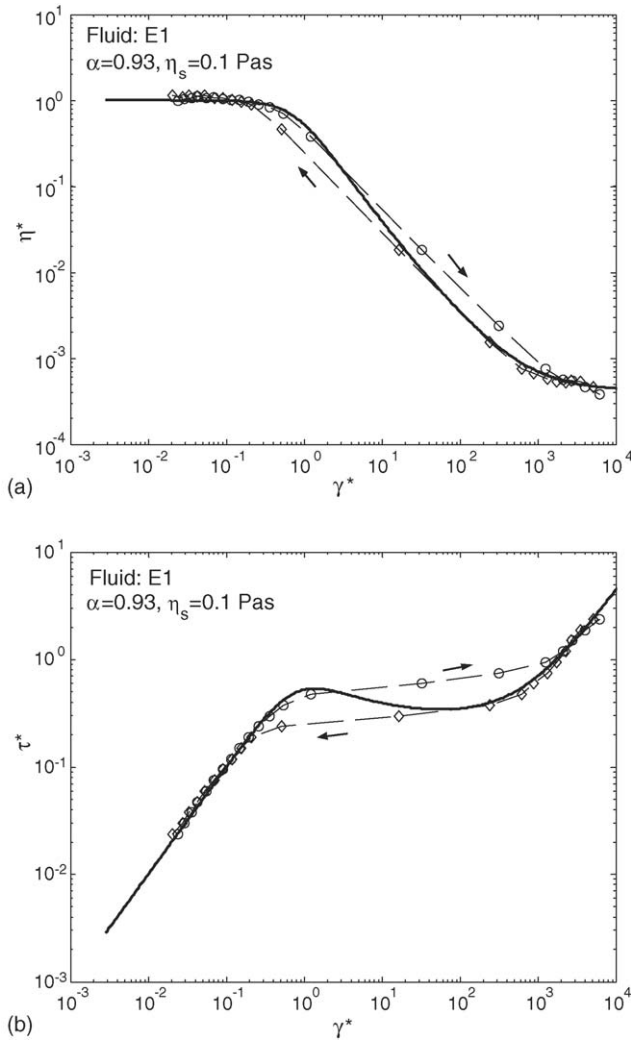
Fig. 5. The results of up and down ramp controlled stress experiments for the E1 fluid: (a) dimensionless viscosity ($\eta^* = \eta/\eta_0$) as function of the dimensionless shear rate ($\gamma^* = \dot{\gamma}\lambda$) and (b) dimensionless stress ($\tau^* = \tau/G_0$) as a function of the dimensionless shear rate. The top branch (hollow circles) corresponds to increasing increments in τ^* and the lower branch (hollow diamonds) to decreasing increments. Solid lines represent results of the single-mode Giesekus constitutive equation (experiments were performed at $T = 25\,^\circ$C).

determined by the top jump condition

$$\tau_{max} \cong 0.67 G_0 \tag{11}$$

as deduced from reptation theory [24]. A marginally smaller value of $\tau_{max} \cong 0.54 G_0$ is predicted for nonuniform flow fields [78]. The critical stress τ_{min}^* of a down ramp experiment should follow a bottom jump condition and result in a hysteresis between the up and down ramp stress plateau as theoretically proposed by Porte et al. [49].

The resulting nonmonotonic stress versus shear rate curve leads for a certain range of stresses $\tau_1^* < \tau^* < \tau_2^*$ to a bifurcation in the flow and the occurrence of nonhomogeneous behavior in the form of shear-bands. This formation of local spatially inhomogeneous shear-bands has been experimentally observed by NMR imaging [79,80], neutron scattering [81,82] and other flow imaging diagnostics [38,83–89].

The occurrence of an underlying nonmonotonic constitutive relationship between the steady shear stress and shear rate can also be directly inferred from the 'up' and 'down' ramp experiments shown in Fig. 5. The microstructural compositions of the shear-banded states are highly degenerate and at a stress level of τ_{max}^* individual regions may be associated with any deformation rate $\gamma_M^* \leq \gamma^* \leq \gamma_2^*$ indicated in Fig. 1. Theories which incorporate a coupling between stress and microstructure are required in order to provide a selection mechanism for these bands [31].

An increase in the externally imposed driving stress and/or the time of imposed shearing leads to progressive destruction of a larger fraction of the wormy micellar (equilibrium) state and formation of an increasing percentage of the shear-disrupted micellar segments. These segments contribute to the second low-viscosity mode that provides the upper Newtonian contribution to the stress. The final stationary flow state can also strongly depend on the flow history of the micellar solution, as reported by Radulescu et al. [90]. As the stress is decreased from the second Newtonian flow regime, which is dominated by the solvent-like contribution to the total stress, the structural buildup of the wormlike micelles starts at the stress minimum τ_{min}^* indicated in Fig. 1.

The Johnson–Segalman (JS) equation [91] has been commonly used to model the nonmonotonic material instability and formation of shear-banding. Greco and Ball [92] suggested a selection criterion for the symmetry breaking of the band distribution, based on the stress distribution in a circular Couette flow. Lu et al. [93] considered planar shear for a JS model with additional diffusive terms. However, preliminary attempts to fit the present shear-flow experiments indicated that the JS model overpredicted the value of ($\tau_{max}^* - \tau_{min}^*$) within a reasonable shear rate range of $\gamma_1^* \leq \gamma^* \leq \gamma_2^*$. A rederivation of the JS model from microstructural considerations in order to obtain a full set of equations with higher order derivative terms and including a conservation equation for the local number density of micelles coupled to the stress equations may improve the predictions [31].

A simple way to capture this behavior is given by a number of semi-empirical constitutive equations comparable to the Johnson–Segalman equation, which incorporate the linear Maxwell model under small strains or strain rates and are expanded to incorporate additional nonlinearities. Examples of appropriate nonlinear constitutive equations include the Phan-Thien and Tanner model [94], the Giesekus model [25,26], the White-Metzner [95] or the Bird-deAiguiar model [96]. These models may all exhibit nonmonotonic shear stress-rate behavior depending on the values of the relevant nonlinear parameters and the background solvent viscosity.

In the following we will use the single-mode Giesekus constitutive equation (Eq. (2)) to model the hysteresis of the shear-banding phenomenon since this equation has already been demonstrated to model the nonlinear properties of wormlike micellar solution in start-up of steady shear flows quite well [28]. The dimensionless viscosity ($\eta^* = \tau^*/\gamma^*$) computed from the single-mode Giesekus equation is given by:

$$\eta^* = \frac{(1-f)^2}{1+(1-2\alpha)f} + \beta_s, \tag{12}$$

$$f = \frac{1 - \sqrt{(\kappa_1 - 1)/\kappa_2}}{1 + (1 - 2\alpha)\sqrt{(\kappa_1 - 1)/\kappa_2}}, \qquad (13)$$

$$\kappa_1 = \sqrt{1 + 16\alpha(1 - \alpha)(\gamma^*)^2}, \qquad (14)$$

$$\kappa_2 = 8\alpha(1 - \alpha)(\gamma^*)^2, \qquad (15)$$

where α and β_s are, respectively, the anisotropy factor and the dimensionless solvent viscosity that dominates the viscosity of the solution at high shear rates. The solid lines in Fig. 5(a and b) represent the predictions of the model with fitting parameters of $\alpha = 0.93$ and $\eta_s = 0.1\,\mathrm{Pa\,s}$ (or $\beta_s = 4.18 \times 10^{-4}$). The parameter β_s has been chosen as an adjustable parameter since the viscosity in the high shear rate regime includes not only the Newtonian solvent but also the additional, undefined contributions of the surfactant molecules in a nonmicellar state. Small deviations of the solution viscosity at high shear rates from the expected complex viscosity (Eq. (9)) of the Rouse-like regime have also been reported by Manero et al. [14]. The linear viscoelastic rheological parameters given for the E1 solution in Table 1 were used in the calculations as starting values for a best fit of the model to the experimental data.

The maximum deviation between experimental values of the linear viscoelastic parameters and the best fit of the model is only 0.32%, as seen in Table 2 below. The agreement between the plateau values of the experimental data and the local minima and maxima of the theoretical curve is very good, especially in predicting the local minimum of the stress during the down ramp of the stress sweep.

The effect of salt–surfactant concentration ratio, C^*, on the hysteresis/shear-band structure can be seen for $C^* = 13.2$ and 16 (fluid samples E2 and E3) in Fig. 6(a and b). The qualitative features of the flow curves for both fluids are similar to the E1 fluid. However, the distance between the upper and lower branch ($\tau_{\max}^* - \tau_{\min}^*$) decreases as C^* increases. Indeed, the magnitude of the anisotropy factor in the Giesekus model provides a direct measure of the width of the hysteresis gap; α decreases from 0.93 for the E1 fluid to 0.89 and 0.85 for the E2 and E3 fluids, respectively (see Table 2). The stabilizing effect of increasing the salt–surfactant concentration C^* on the micellar fluid structure was also noted by Raghavan and Kaler [11] and was interpreted as a promotion of the level of micellar branching. The specific details of the range of salt–surfactant concentration required for phase-stabilization is expected to vary with the nature of the counterion (e.g. whether it is binding or nonbinding). However, there is at present no reported microstructural analysis
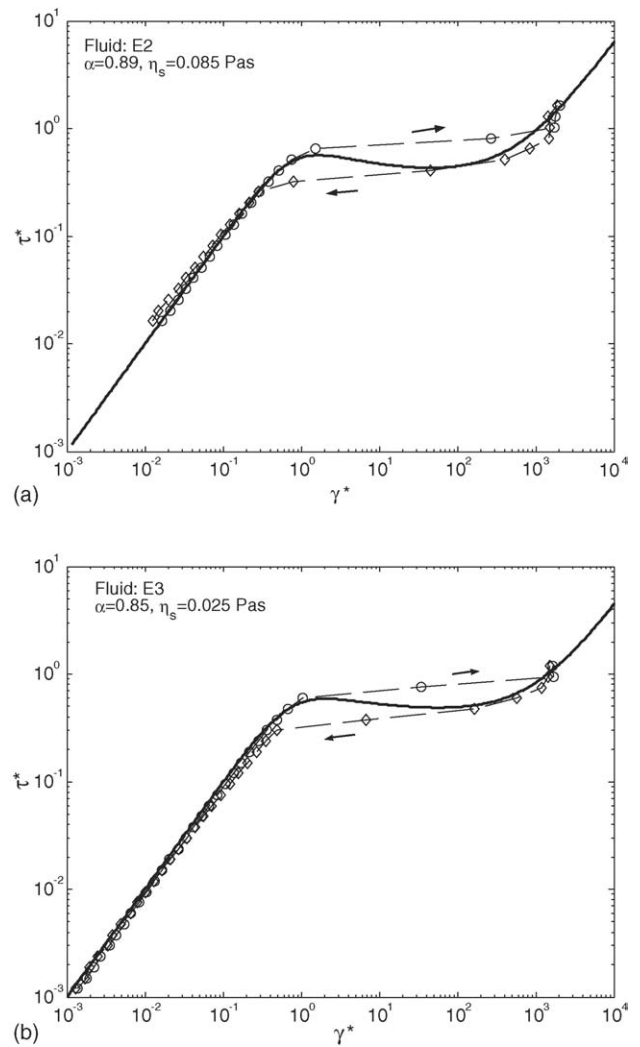

Fig. 6. The results of up and down ramp controlled stress experiments: (a) for the E2 fluid ($C^* = 13.2$) and (b) for the E3 fluid ($C^* = 16$). Solid lines represent the Giesekus model predictions (experiments were performed at $T = 25\,^\circ\mathrm{C}$).

and phase behavior data for the current samples to confirm this hypothesis.

The observable range of the Newtonian regime after the second upturn in the shear stress also becomes smaller with increasing C^* due to a fast transition of the micellar solution to a foamy thixotropic state that shows a strong increase of the shear stress at a nearly constant rate. The stress sweep experiments cannot proceed further since irreversible structural changes occur at higher stresses. This stress-jump behavior at the transition to a shear induced structure [34,44] limits the ability of the single-mode Giesekus equation to model the macroscopic stress beyond the shear-banding regime because the solution is no longer a single homogeneous phase. All of our experiments are truncated at this SIS transition.

The effects of temperature on the dynamics of shear-banding were also investigated for the E1 fluid over a temperature range of 25–70 °C. The required zero shear viscosities for evaluation of the Giesekus model predictions were obtained from time-temperature superposition. The temperature dependent shift factor $a_T(T; T_0)$ was determined from a series of ten viscosity
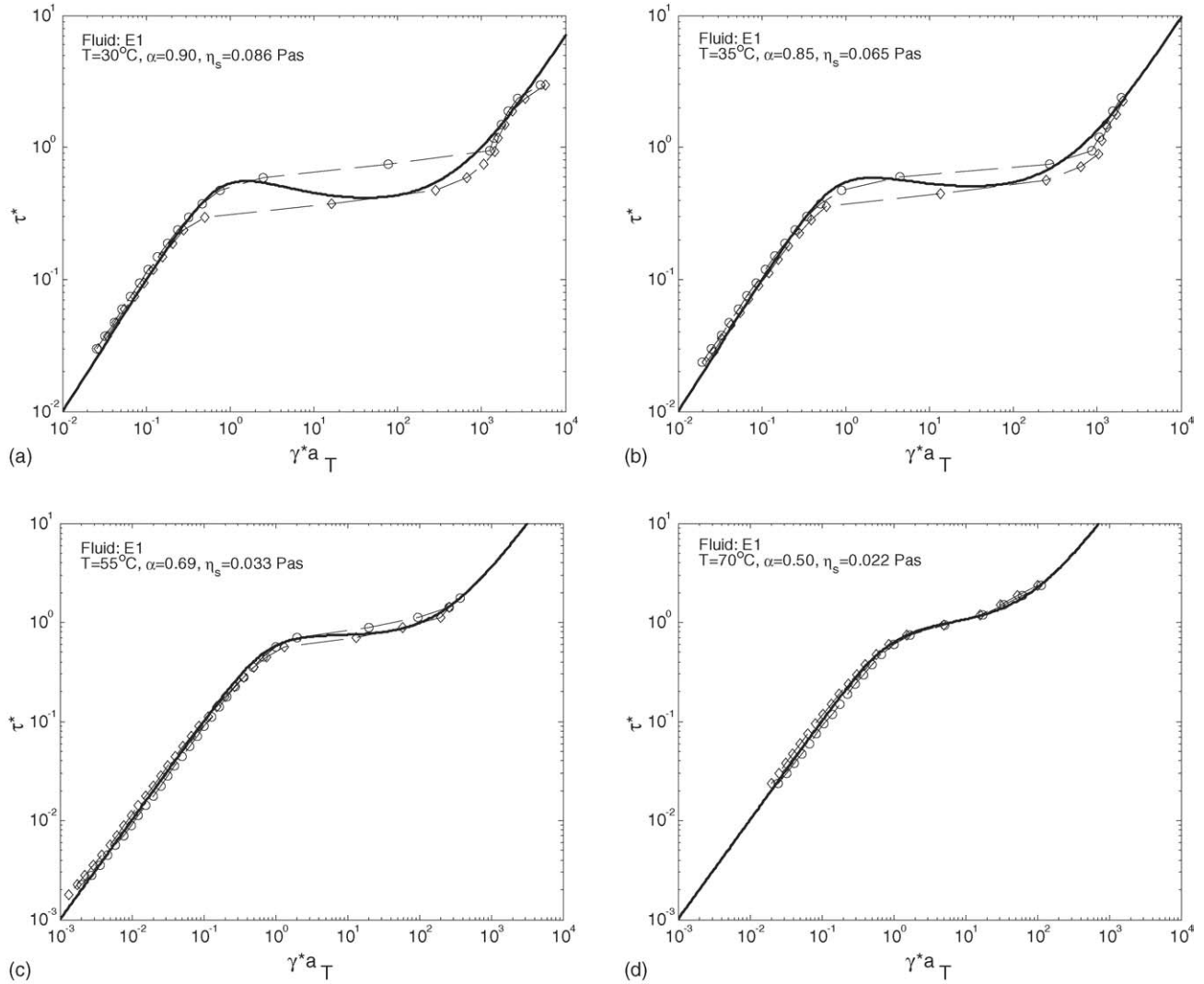
Table 2
Giesekus model parameters in shear flow ($T = 25\,^\circ\mathrm{C}$)

	E1	E2	E3
λ (s)	28.4 (0.07)[a]	11.6 (6.6)	4.97 (−0.6)
G_0 (Pa)	8.42 (0.24)	12.3 (6.2)	12.6 (6.4)
η_0 (Pa s)	239 (0.32)	143 (13.2)	62.4 (5.7)
α	0.93	0.89	0.85
η_s (Pa s)	0.10	0.085	0.025

[a] The numbers in parentheses show deviation (in percentage) from linear rheology experiments.

Fig. 7. Influence of the temperature on hysteresis/shear-band structure for the E1 fluid: (a) $T = 30\,^{\circ}$C, (b) $T = 35\,^{\circ}$C, (c) $T = 55\,^{\circ}$C and (d) $T = 70\,^{\circ}$C. Solid lines represent the Giesekus model fits at each temperature.

measurements over low shear rates ($\gamma^* \le \gamma_1^*$) in a temperature range of $25\,^{\circ}\text{C} \le T \le 70\,^{\circ}\text{C}$ and a_T follows a simple activated rate process of Arrhenius form

$$a_\text{T}(T) = \frac{\eta(\dot{\gamma}, T)}{\eta(\dot{\gamma}, T_0)} \frac{T_0 \rho(T_0)}{T \rho(T)} \approx \exp\left[\frac{\Delta H}{R}\left(\frac{1}{T} - \frac{1}{T_0}\right)\right] \quad (16)$$

where a_T is the temperature shift function and the density ratio $\rho(T_0)/\rho(T)$ for the aqueous micellar solution is assumed to be approximately equal to unity over the investigated temperature range. For the investigated system with $T_0 = 25\,^{\circ}$C, the activation energy ratio $\Delta H/R$ was found to be 11500 K. The thermal variations of the background solvent viscosity $\eta_\text{s}(T)$ and anisotropy factor $\alpha(T)$ were determined by an independent fitting procedure. The variation of these parameters with temperature is also found to be nearly exponential. The experimental and model results are given in Fig. 7. The hysteretic behavior becomes progressively weaker at elevated temperatures, and finally disappears at $70\,^{\circ}$C. The anisotropy factor α in the Giesekus model clearly confirms this trend and decreases from 0.93 at $T = 25\,^{\circ}$C to 0.50 at $70\,^{\circ}$C. The value $\alpha = 0.5$ corresponds to the Leonov model and is the

limiting value between a monotone rise of the stress (with the absence of the hysteresis behavior) and the development of a shear-banding region [97].

Visual analysis also shows that the fluid sample remains homogeneous and rheological data can be measured up to $90\,^{\circ}$C. The stabilizing effect of a moderate level of temperature rise has previously been observed for viscoelastic flow instabilities [98,99]. There are also computational studies in the context of elastic instabilities to confirm this observation. For EHAC based solutions, the effect of temperature on the degree of micellar branching is shown to be analogous to increases in salt concentration [12], and hence such a stabilization effect with increasing temperature is to be expected.

3.2.2. Transient shear flow

The temporal characteristics of the nonmonotone stress shear rate relation and the hysteresis behavior of the viscoelastic surfactant solution in circular Couette flow can be monitored by following the transient shear rate evolution at various values of a constant controlled shear stress.
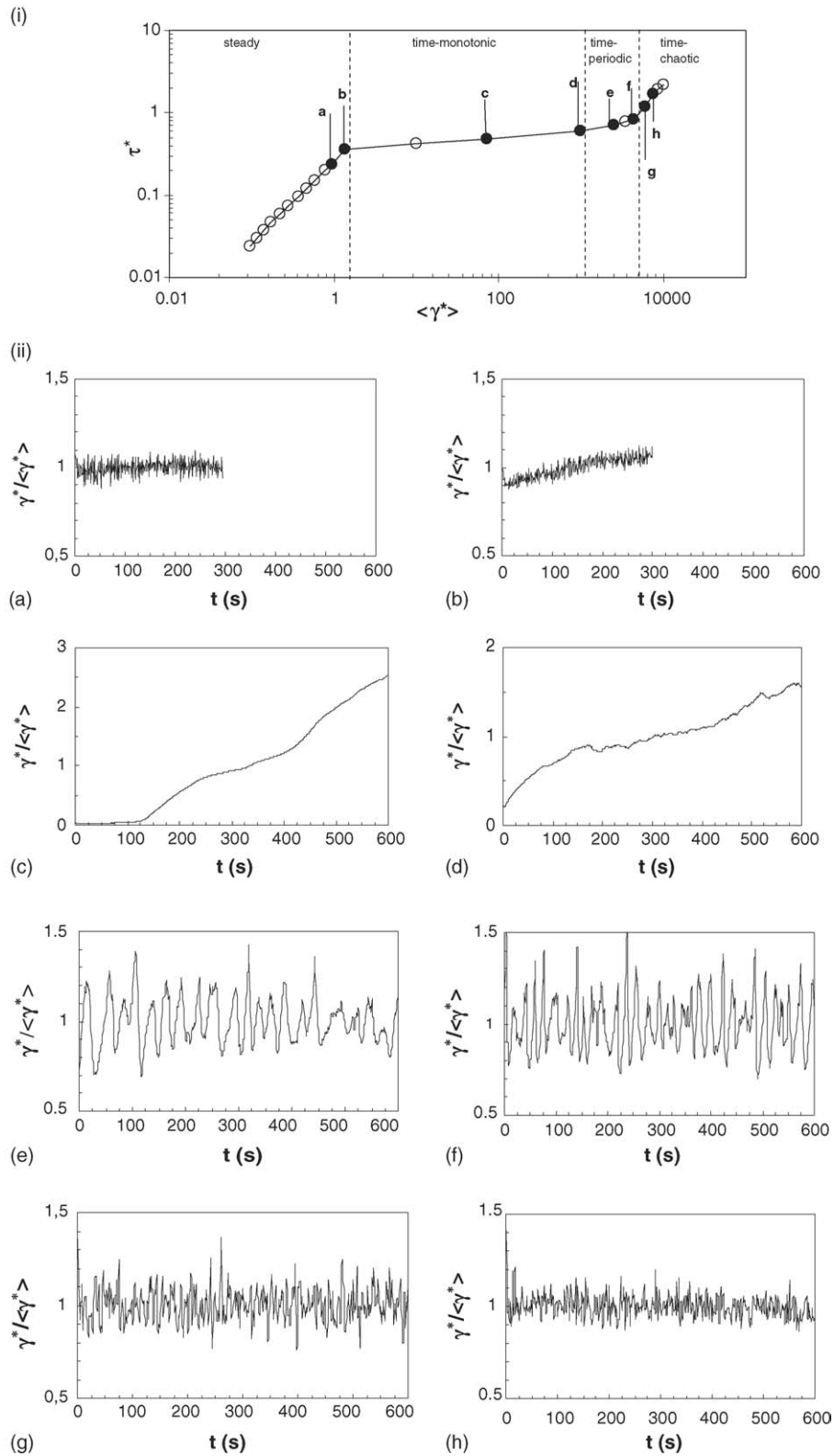
Fig. 8. Measurements of temporal fluctuations in the shear rate for various values of the dimensionless shear stress for the E1 fluid. Each transient shear rate $\gamma^*(t)$ at a given τ^* is normalized by the corresponding time-averaged nominal value ($\langle\gamma^*(t)\rangle$): (i) location of the transient experiments on the qualitative stress shear rate curve and (ii) transient shear rates for various values of (τ^*; $\langle\gamma^*(t)\rangle$): (a) (0.36; 0.95) (b) (0.42; 1.37), (c) (0.48; 81), (d) (0.60; 1382), (e) (0.72; 3318), (f) (0.84; 3719), (g) (1.2; 4778) and (h) (1.68; 5514) (experiments were performed at $T = 25\,°C$).

A series of measurements of the evolution in the transient dimensionless shear rate of $\gamma^*(t)$ is shown (for E1 fluid) in Fig. 8 for various values of the dimensionless shear stress, τ^*. The dimensionless shear rate $\gamma^*(t)$ is normalized by its time-averaged nominal value ($\langle\gamma^*(t)\rangle$) to illustrate the relative magnitude of the fluctuations around unity. For low values of τ^*, the instantaneous shear rate is essentially constant in time (t), as shown in Fig. 8(a and b) with r.m.s. fluctuations of less than 4.2 and 4.1%, respectively. For $\tau^* < 0.48$ the shear flow of the micellar solution is steady. The flow becomes strongly time-dependent as the dimensionless stress is increased to $\tau^* = 0.48$, as depicted in Fig. 8(c). The shear rate monotonically increases with time over the time range of the experiment. The experimental timescale is restricted to about 600 s at each stress to minimize the effect of evaporation of the sample in a longer time-period. Grand et al. [78] noted that at the onset of the plateau region the timescale for equilibration into the final steady state could be up to two orders of magnitude higher than the linear viscoelastic relaxation time. This monotonic increase of the shear rate with time continues even at higher values of τ^* (see Fig. 8(d)) in the nearly horizontal plateau regime of the τ^*–γ^* plot. Eventually, this transient increase of the shear rate saturates into a strongly time-periodic flow around an average shear rate as seen in Fig. 8(e and f) at the upper end of the plateau regime. The amplitude of the shear rate fluctuations in this time-periodic flow state can reach up to 50% with respect to the nominal value (or up to 14.8% in terms of r.m.s. fluctuations). At the highest stresses ($\tau^* \approx 1$), on the upper branch of the flow curve corresponding to Fig. 8(g and h), the fluctuations decrease again and are less than, respectively, 15 and 10% (or 9 and 6% in r.m.s. fluctuations) of the nominal signal.

The characteristic frequencies of the shear rate oscillations can be quantitatively identified by Fourier analysis of the time series measurements. Power spectral-densities of $\gamma^*(t)$

are shown in Fig. 9 for selected values of τ^*. Fig. 9(a–d), respectively correspond to power spectral densities of the signals $\gamma^*(t)/\langle\gamma^*(t)\rangle$ given in Fig. 8(e–h). The power spectrum obtained from FFT analysis are also normalized by a nominal component of the spectrum for each τ^*, in order to provide consistency in comparison, as suggested by Yesilata et al. [100]. For $\tau^* = 0.72$, the power spectrum shows a peak at $f_1 = 0.032$ Hz (Fig. 9(a)), corresponding to a dimensionless frequency value of $f_1^* = \lambda f_1 \approx 1$ since the characteristic relaxation time of the fluid is $\lambda = 28.4$ s. The nominal steady rotation rate of the Couette fixture is $\omega_c = \langle\dot{\gamma}\rangle/\Lambda = 2.6$ rad/s, where $\Lambda = R_1/d$ is the ratio of inner rotor radius to the gap [101]. The nominal rotation rate is thus nearly one order higher than the value of $\omega_1 = 2\pi f_1 = 0.2$ in rad/s. Wheeler et al. [38] performed similar experiments using a controlled stress device at a nominally constant deformation rate between $\gamma_M^* \leq \gamma^* \leq \gamma_m^*$. In their experiments, strongly periodic oscillations were observed above a critical stress with a frequency that was dependent on the moment of inertia of the test (Couette) fixture and the characteristics of the instrument feedback loop. We see no such coupled instrument/fluid oscillations with the present rheometer (probably due to a tighter feedback control loop). The periodic frequency identified in Fig. 9(a) corresponds purely to the fluctuating material response since the dimensionless frequency is nearly equal to unity ($f_1^* \approx 1$).

For stresses above the critical value for onset of time-periodic flow, the dominant frequency of oscillations increases and multiple peaks are discernable (Fig. 9(b)). The appearance of these new peaks in the power spectrum can be considered as the first sign of the onset of a more complex chaotic-like flow. In the strongly fluctuating regimes shown in Fig. 9(c and d) the shear rate oscillates with multiple in commensurate frequencies as determined by the FFT analysis. However, the intensity of the oscillations decreases, as the linear relationship between
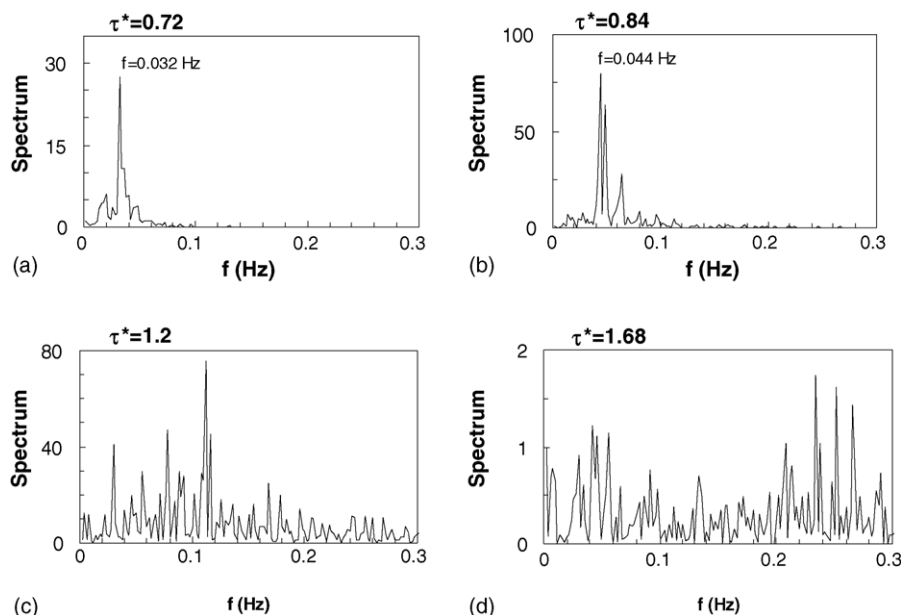

Fig. 9. Fast Fourier transforms (FFT) of $\gamma^*(t)$ in the time-periodic and the time-chaotic regions for E1 fluid. The corresponding dimensionless stresses are given as: (a) $\tau^* = 0.72$, (b) $\tau^* = 0.84$, (c) $\tau^* = 1.20$ and (d) $\tau^* = 1.68$. The spectra are normalized with the nominal value of the spectrum for each case.

τ^* and $\langle \gamma^*(t) \rangle$ is re-established and the stress shear rate curve approaches the second upper linear flow regime.

The time-dependent fluctuations leading to inhomogeneous and banded structures were noted recently by Lee et al. [39] in the middle of the gap of a Couette cell using pointwise flow-induced birefringence (FIB) measurements. Recent studies have shown that transient oscillations also occur in more complex flows of micellar fluids with shearing and extensional kinematics [52,53]. It does appear that these fluctuations are not specific to a single kinematic field but are common to all flows in which the characteristic deformation rate and micellar time scale are on the same order.

3.3. Transient extensional flow of micellar solutions

The transient extensional response of three micellar fluids (E1, E2 and E3) was also investigated with a capillary breakup extensional rheometer. The experimental device utilizes plates of radius $R_0 = 3.0$ mm separated by an initial distance $L_0 = 2.2$ mm so that the initial aspect ratio is $\Lambda_0 = L_0/R_0 = 0.733$. The plates are separated rapidly (within 50 ms) to a final separation of $L_1 = 6.6$ mm.

Fig. 10 shows a sequence of images of the test fluids at $T = 25\,^\circ$C. The first images show that the initial filament configu-

(a) Fluid: E1

t=0   t=18.25s   t=36.5s   t=54.75s   t=73s

(b) Fluid: E2

t=0   t=6s   t=12 s   t=18s   t=24s

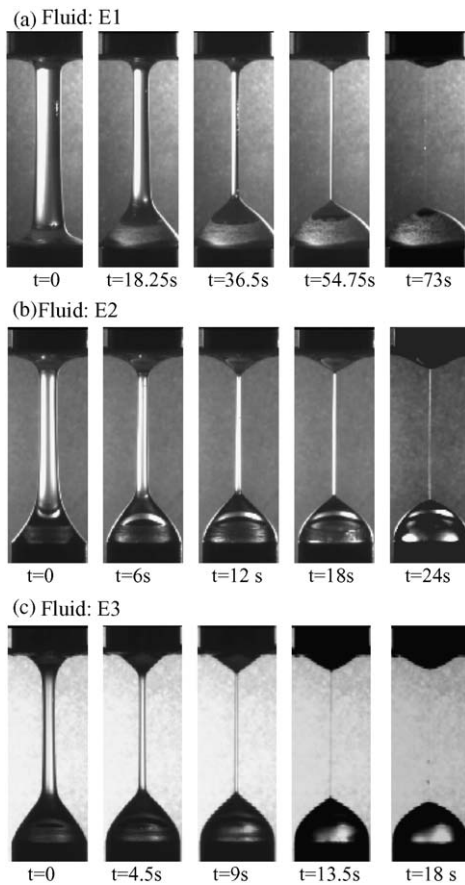(c) Fluid: E3

t=0   t=4.5s   t=9s   t=13.5s   t=18 s

Fig. 10. Time-sequences of flow images in the CABER experiments for (a) E1 fluid ($C^* = 10.6$), (b) E2 fluid ($C^* = 13.2$) and (c) E3 fluid ($C^* = 16$) (experiments were performed at $T = 25\,^\circ$C).

rations for all samples are axially nonuniform. For convenience, time is referenced to the instant when stretching is halted (i.e. we set $t = t_1 = 0$). The subsequent images show the progressive elasto-capillary drainage and ultimate breakup of the filament at a critical time after the cessation of stretching. The temporal resolution of the breakup event is limited by the framing rate of the video camera to 30 frames/s.

The filaments of all three samples shown in Fig. 10 neck and break in a quantitatively different manner. Both the axial profiles of the filaments and the time evolution in the midfilament diameter are significantly different for each type of fluid. The axial profile of the E1 fluid filament is nearly homogeneous, and the minimum diameter is always close to the midplane (although gravitational effects cause the actual minimum to be slightly above the midplane at initial stages). The effect of gravity at early times becomes more pronounced for the E2 sample, and especially for the E3 fluid. However, at later stages, the axial profile of the filament rapidly evolves into an axially uniform cylindrical filament. The time to breakup for the E1 fluid is significantly longer than those of E2 and E3.

Transient midfilament diameters measured for the three fluids are shown in Fig. 11(a). Notice that measurements from three separate experiments for each fluid agree extremely well and we obtain excellent experimental reproducibility. Measurements of the filament evolution for the fluids decay approximately exponentially with time as shown by the solid lines. Prior to the breakup, significant deviation from the initial exponential curve occurs caused by the finite extensibility of the micellar structures.

Entov and Hinch [67] have shown that the exponential behavior of the midfilament thinning at intermediate times is related to a balance of the capillary and elastic forces in the thread and allows for the calculation of a relaxation time λ_E in the elongational flow,

$$D_{\text{mid}}(t) \sim \exp\left[-\frac{t}{3\lambda_E} \right]. \tag{17}$$

For Boger fluids, Anna and McKinley [66] confirmed (in accordance with the theoretical predictions from Entov and Hinch [67]) that $\lambda_E \approx \lambda$, where λ is the longest relaxation time of the polymer solution determined from linear viscoelastic measurements. However, in these micellar fluids, the characteristic relaxation times for transient elongation, extracted from the linear regimes in the semi-logarithmic plots in Fig. 11(a) according to Eq. (17) and shown in Table 3, are substantially lower (by

Table 3
Giesekus model parameters in extensional flow ($T = 25\,^\circ$C)

	E1	E2	E3
λ_E (s)	9.03	3.63	1.65
G_0 (Pa)	7.98 (−5.0)[a]	11.5 (−0.52)	11.9 (1.62)
η_0 (Pa s)	215 (−9.71)	125 (−0.71)	59.5 (0.97)
η_s (Pa s)	0.10	0.085	0.025
α	0.02	0.031	0.003
a	0.229	0.241	0.227

[a] The numbers in parentheses show deviation (in percentage) from linear rheology experiments.
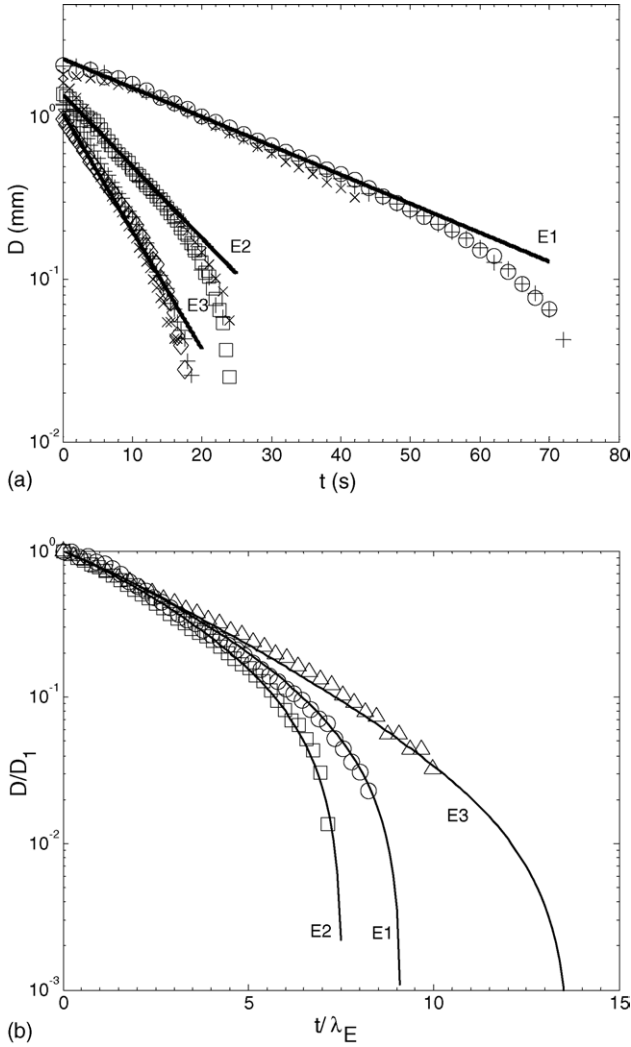
Fig. 11. (a) Transient midfilament diameter profiles of the E1, E2 and E3 fluids. Different symbols correspond to separate CABER experiments for each fluid. Solid lines show best exponential fits of the curves. (b) Comparison of measured midfilament diameter profiles (symbols) for micellar fluid filaments with predictions from the single-mode Giesekus model (solid lines). The diameter and time are scaled with D_1 and λ_E (experiments were performed at $T = 25\,^\circ$C).

almost a factor of three) than the relaxation times obtained from oscillatory shear flow. We are not aware of any other reports of the characteristic time constant for extensional flow of micellar solutions; however, Rothstein [65] noted that the apparent nonlinearity of a micellar network is also characterized by very different values of the relevant rheological parameter in shear and extension (in this case the finite extensibility parameter). This factor of three differences in the characteristic relaxation time must be associated with the different dynamics of micelle creation and destruction in the elongated and aligned state that is associated with extensional flow in a thinning filament as compared to the fully entangled three-dimensional structure that exists under equilibrium conditions. Thus, the transient extensional behavior of the wormlike micelles studied here appears to be more complex than that expected for a simple viscoelastic fluid of Maxwell–Oldroyd type.

We now use the simple zero-dimensional formulation proposed by Entov and Hinch [67] to predict the filament thinning behavior of the micellar fluid samples using the single-mode Giesekus constitutive equation. Ignoring axial curvature effects, the temporal evolution of the filament mid-diameter D_{mid} is given by a balance of the viscous, elastic and capillary forces (see Anna and McKinley [66]):

$$\frac{dD_{mid}}{dt} = \frac{1}{6\eta_s}[(\tau_{zz} - \tau_{rr})D_{mid} - 2\sigma] \qquad (18)$$

where σ denotes the surface tension of the fluid and τ_{zz} and τ_{rr} are the additional micellar contributions to the axial and radial tensile stress components of the total stress tensor τ.

For an ideal uniaxial extensional flow, these stress components are evaluated from the Giesekus constitutive equation (Eq. (2)), which becomes

$$\lambda_E \frac{d\tau_{zz}}{dt} + (1 - 2\dot{\varepsilon}\lambda_E)\tau_{zz} + \frac{\alpha}{G_0}\tau_{zz}^2 = 2G_0\lambda_E\dot{\varepsilon} \qquad (19)$$

$$\lambda_E \frac{d\tau_{rr}}{dt} + (1 + \dot{\varepsilon}\lambda_E)\tau_{rr} + \frac{\alpha}{G_0}\tau_{rr}^2 = -G_0\lambda_E\dot{\varepsilon} \qquad (20)$$

where the rate of strain is expressed by

$$\dot{\varepsilon} = -\frac{2}{D_{mid}}\frac{dD_{mid}}{dt}. \qquad (21)$$

Combining Eq. (18) with Eqs. (19)–(21) gives a coupled set of ordinary differential equations (ODEs) for D_{mid}, τ_{zz} and τ_{rr}. The Eqs. (18)–(20) can be integrated using standard routines for stiff ODEs under appropriate initial conditions. The corresponding initial conditions when the stretching is halted are given by [66]:

$$D_{mid}(t_1 = 0) = D_1, \qquad (22)$$

$$\tau_{zz}(t_1 = 0) \cong \frac{2\sigma}{D_1} - a\frac{2\eta_s}{\lambda_E}, \qquad (23)$$

$$\tau_{rr}(t_1 = 0) = 0. \qquad (24)$$

The parameter a in Eq. (23) has been introduced by Anna and McKinley [66] to correctly account for the initial deformation. The results of simulations (the solid lines), using a and α as adjusting parameters, along with experimental measurements (the symbols) are depicted in Fig. 11(b). The time and diameter are scaled with λ_E and D_1, respectively, and the parameters used in the calculations are listed in Table 3. It can be seen from the figure that quantitative agreement between experiments and theoretical predictions can be obtained, provided that the model parameters are not forced to be the same as the values obtained in shear flow. The anisotropy factor α for extensional flows obtained from the fits is more than a decade smaller than the value for shear experiments (see Table 2). Most interestingly, the relaxation times λ_E obtained from best fits to Eq. (17) are a factor of almost three smaller than the value expected in shear flow. This suggests that the arguments leading to Eq. (4) for λ need to be modified for an elongated micellar chain reptating and breaking/reforming in an extensional flow.

It is also desirable to re-express the midfilament diameter data in a more intuitive format, i.e. as a transient tensile stress or

extensional viscosity. The thinning dynamics of the elastic fluid filaments result from an interplay between the fluid rheology and the effects of capillarity. We have demonstrated that the observed evolution of the midfilament diameter as the fluid thread necks down and breaks can be well described using a single-mode Giesekus model and an appropriate force balance on the fluid filament, provided that the initial deformation is correctly accounted for. The transient extensional rheology of the fluid is encoded in this evolution and we can obtain an apparent extensional viscosity that is related directly to the midfilament diameter by using the same approach described by Anna and McKinley [66]. An appropriate apparent extensional viscosity calculated from the surfactant and solvent contributions is given by

$$\eta_E = \frac{(\tau_{zz} - \tau_{rr})}{\dot{\varepsilon}} + 3\eta_s. \tag{25}$$

This relation combined with Eq. (18) and (21) gives a direct dependence of the apparent extensional viscosity from the mid-filament diameter evolution

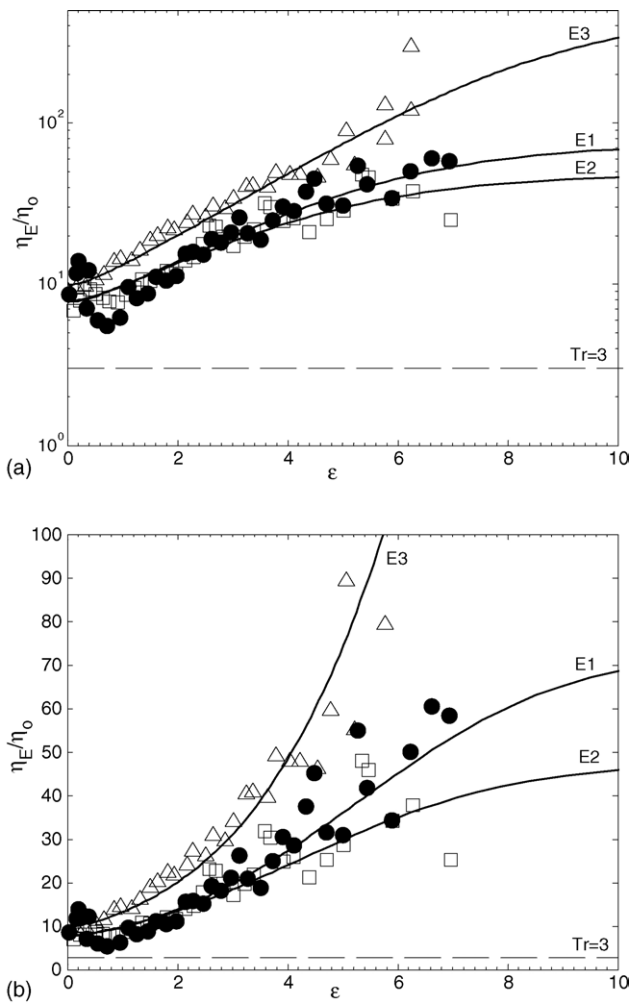$$\eta_E = -\frac{\sigma}{\frac{dD_{mid}}{dt}} \tag{26}$$

(a)

(b)

Fig. 12. Comparison of apparent extensional viscosities computed from mid-filament diameter profiles of E1 (●), E2 (□) and E3 (△) fluids, along with predictions from the single-mode Giesekus model (solid lines): (a) in log-scale and (b) in linear-scale.

and we thus differentiate the experimental diameter data to obtain the transient extensional viscosity. The results are presented in Fig. 12 and show the apparent extensional viscosity in terms of a dimensionless Trouton ratio (η_E/η_0) as a function of the total Hencky strain ε

$$\varepsilon = 2 \ln \left[\frac{D_1}{D_{mid}(t)} \right]. \tag{27}$$

The experimental diameter data obtained from Eq. (26) are shown as symbols and the Giesekus simulations are indicated by solid lines. In general, the experimental and theoretical values for the apparent extensional viscosities extracted from elasto-capillary thinning agree well for all three samples. The extensional viscosity at time t_1 is a factor of approximately three higher than the expected extensional viscosity of $3\eta_0$ from the Trouton ratio due to the initial stretch that is imposed by the rapid extension to the final plate separation prior to the surface tension driven filament thinning. The extensional viscosity asymptotically reaches a steady state value when the strain becomes large. However, the final approach to breakup falls below the calibrated minimum resolution of 20 μm of the CABER device. The observed Trouton ratios approaching this steady state are on the order of 100. Rothstein [65] obtained a similar magnitude increase in the Trouton ratio for a wormlike micellar solution system (CTAB/NaSal) in a constant rate filament stretching experiment at constant deformation rate of $\dot{\varepsilon} \cong 1.55\,\mathrm{s}^{-1}$.

4. Conclusions

In the present study, we have examined the linear viscoelasticity, nonlinear shear and extensional flow dynamics for the ternary system of EHAC/NH$_4$Cl in salt-free water. EHAC based wormlike micellar solutions are relatively new materials in the context of wormlike micellar structures and the linear viscoelastic properties have recently been investigated [11,12] in the presence of different counterions (NaSal, NaCl and NaTos). The present experiments confirm the earlier observations that EHAC-based solutions are highly viscoelastic and their structure and rheology delicately depend on the chemical structure and the amount of salt used as counterion and on the surfactant concentration and temperature. Although the zero shear rate viscosities of our solutions at room temperature can be two to three orders of magnitude lower than those studied previously using different salts, similar nonmonotonic trends in the linear viscoelastic properties are obtained. As shown in Figs. 2 and 3, the solutions are well-described by a single-mode Maxwell response at low frequencies ($\omega \lesssim 1/\lambda$), but some significant deviations from this behavior at intermediate and high frequency regimes are observed for $5.2 \leq C^* \leq 8$. The variations of the zero shear viscosity and relaxation time as a function of salt concentration are nonmonotonic as indicated in Fig. 4. These nonmonotonic rheological responses are not observed in all micellar fluids and have been attributed to the long, unsaturated chains and complex headgroups of EHAC-based surfactants [11].

Stepped shear flow experiments reveal the hysteretic behavior of these wormlike micellar fluid samples upon increasing and decreasing shear stress. This hysteresis can be interpreted

as an indication of a nonmonotonic underlying flow curve and
the onset of shear-banding at intermediate shear rates. At low
and high shear rates outside this shear-banding regime, the flow
curves measured upon increasing and decreasing shear stress
coincide. The nonmonotonic hysteretic behavior can be modeled
with a single-mode Giesekus constitutive equation, provided that
the anisotropy factor α is greater than 0.5. The hysteretic behav-
ior was investigated under a number of different conditions;
increasing values of salt concentration narrow the hysteresis
region as does an increase in the solution temperature.

The transient evolution of the viscoelastic surfactant solu-
tion in steady Couette flow under controlled stress conditions
was explored by conducting a series of instantaneous shear rate
measurements over a wide range of shear stresses. The critical
conditions for the onset of time-dependent flow were determined
quantitatively from these measurements and coincide with the
range of stresses for which hysteretic behavior in the flow curve
is observed.

Experimental observations of the extensional flow behavior
of the micellar fluid samples in capillary breakup experiments
show strong extensional thickening of the samples with the
apparent Trouton ratios increasing by up to two orders of magni-
tude. The characteristic relaxation times of the fluids determined
from extensional flow experiments are consistently lower than
expected from oscillatory shear flow experiments. A comparison
of the extensional experiments with predictions computed using
the single-mode Giesekus model show good quantitative agree-
ment, however, much lower anisotropy factors (α) are required.

It is thus clear that although a simple nonlinear network
model, such as the Giesekus model captures many of the global
features of wormlike micellar rheology it is not (presently) capa-
ble of accurately reflecting the changes in micelle structure that
arise when the kinematics are changed. A more detailed micro-
scopic analysis of the network creation and destruction processes
thus appears warranted. We hope to report on this in the future.

Acknowledgements

References

[1] R.G. Larson, The Structure and Rheology of Complex Fluids, Oxford University Press, New York, 1999.
[2] M.T. Truong, L.M. Walker, Quantifying the importance of micellar microstructure and electrostatic interactions on the shear-induced struc-tural transition of cylindrical micelles, Langmuir 18 (2002) 2024–2031.
[3] Z.Q. Lin, J.L. Zakin, Y. Zheng, H.T. Davis, L.E. Scriven, Y. Talmon, Comparison of the effects of dimethyl and dichloro benzoate counte-rions on drag reduction, rheological behaviors, and microstructures of a cationic surfactant, J. Rheol. 45 (2001) 963–981.
[4] W. Wei, E.S. Yeung, DNA capillary electrophoresis in entangled dynamic polymers of surfactant molecules, Anal. Chem. 73 (2001) 1776–1783.
[5] W.J. Kim, S.M. Yang, Flow-induced silica structure during in situ gelation of wormy micellar solutions, Langmuir 16 (2000) 4761–4765.
[6] J. Yang, Viscoelastic wormlike micelles and their applications, Curr. Opin. Colloid Interface Sci. 7 (2002) 276–281.
[7] B. Chase, W. Chmilowski, R. Marcinew, C. Mitchell, Y. Dang, K. Krauss, E. Nelson, T. Lantz, C. Parham, J. Plummer, Clear fracturing fluids for increased well productivity, Oilfield Rev. 9 (1997) 20–33.
[8] G.C. Maitland, Oil and gas production, Curr. Opin. Colloid Interface Sci. 5 (2000) 301–311.
[9] M.M. Samuel, Methods of fracturing subterranean formations, USA, 6,306,800.
[10] M.M. Samuel, R.J. Card, E.B. Nelson, J.E. Brown, P.S. Vinod, H.L. Temple, Q. Qu, D.K. Fu, Polymer-free fluid for fracturing applications, SPE Drill. Complet. 14 (1999) 240–246.
[11] S.R. Raghavan, E.W. Kaler, Highly viscoelastic wormlike micellar solutions formed by cationic surfactants with long unsaturated tails, Langmuir 17 (2001) 300–306.
[12] S.R. Raghavan, H. Edlund, E.W. Kaler, Cloud-point phenomena in wormlike micellar systems containing cationic surfactant and salt, Langmuir 18 (2002) 1056–1064.
[13] B.A. Schubert, N.J. Wagner, E.W. Kaler, S.R. Raghavan, Shear-induced phase separation in solutions of wormlike micelles, Langmuir 20 (2004) 3564–3573.
[14] O. Manero, F. Bautista, J.F.A. Soltero, J.E. Puig, Dynamics of worm-like micelles: the Cox–Merz rule, J. Non-Newtonian Fluid Mech. 106 (2002) 1–15.
[15] V. Croce, T. Cosgrove, G. Maitland, T. Hughes, G. Karlsson, Rheology, cryogenic transmission electron spectroscopy, and small-angle neutron scattering of highly viscoelastic wormlike micellar solutions, Langmuir 19 (2003) 8536–8541.
[16] L.M. Walker, Rheology and structure of worm-like micelles, Curr. Opin. Colloid Interface Sci. 6 (2001) 451–456.
[17] W. Richtering, Rheology and shear induced structures in surfactant solutions, Curr. Opin. Colloid Interface Sci. 6 (2001) 446–450.
[18] L.J. Magid, The surfactant-polyelectrolyte analogy, J. Phys. Chem. B 102 (1998) 4064–4074.
[19] M.E. Cates, Nonlinear viscoelasticity of wormlike micelles (and other reversibly breakable polymers), J. Phys. Chem. 94 (1990) 371–375.
[20] R. Granek, M.E. Cates, Stress-relaxation in living polymers: results from a poisson renewal model, J. Chem. Phys. 96 (1992) 4758–4767.
[21] M.S. Turner, M.E. Cates, Linear viscoelasticity of living polymers: a quantitative probe of chemical relaxation-times, Langmuir 7 (1991) 1590–1594.
[22] F. Kern, F. Lequeux, R. Zana, S.J. Candau, Dynamical proper-ties of salt-free viscoelastic micellar solutions, Langmuir 10 (1994) 1714–1723.
[23] M.E. Cates, Reptation of living polymers: dynamics of entangled polymers in the presence of reversible chain-scission reactions, Macro-molecules 20 (1987) 2289–2296.
[24] N.A. Spenley, M.E. Cates, T.C.B. McLeish, Nonlinear rheology of wormlike micelles, Phys. Rev. Lett. 71 (1993) 939–942.
[25] H. Giesekus, A simple constitutive equation for polymer fluids based on the concept of deformation-dependent tensorial mobility, J. Non-Newtonian Fluid Mech. 11 (1982) 69–109.
[26] H. Giesekus, A unified approach to a variety of constitutive models for polymer fluids based on the concept of configuration-dependent molecular mobility, Rheol. Acta 21 (1982) 366–375.
[27] P. Fischer, H. Rehage, Non-linear flow properties of viscoelastic sur-factant solutions, Rheol. Acta 36 (1997) 13–27.
[28] T. Holz, P. Fischer, H. Rehage, Shear relaxation in the nonlinear-viscoelastic regime of a Giesekus fluid, J. Non-Newtonian Fluid Mech. 88 (1999) 133–148.
[29] M. Pflaumbaum, H. Rehage, Myristyl dimethylamine oxide surfactant solutions: model systems for rheological research, Eur. J. Chem. Phys. Phys. Chem. 4 (2003) 705–713.

[30] T.C.B. McLeish, R.C. Ball, A molecular approach to the spurt effect in polymer melt flow, J. Polym. Sc. Part B: Polym. Phys. 24 (1986) 1735–1745.

[31] L.P. Cook, L.F. Rossi, Shear layers and demixing in a model for shear flow of self-assembling micellar solutions, J. Non-Newtonian Fluid Mech. 116 (2004) 347–369.

[32] J.K.G. Duhont, A constitutive relation describing the shear-banding transition, Phys. Rev. E 60 (1999) 4534–4544.

[33] P.D. Olmsted, Dynamics and flow-induced phase separation in polymeric fluids, Curr. Opin. Colloid Interface Sci. 4 (1999) 95–100.

[34] C.H. Liu, D.J. Pine, Shear-induced gelation and fracture in micellar solutions, Phys. Rev. Lett. 77 (1996) 2121–2124.

[35] J.F. Berret, D.C. Roux, P. Lindner, Structure and rheology of concentrated wormlike micelles at the shear-induced isotropic-to-nematic transition, Eur. Phys. J. B 5 (1998) 67–77.

[36] V. Schmitt, C.M. Marques, F. Lequeux, Shear-induced phase-separation of complex fluids: the role of flow-concentration coupling, Phys. Rev. E 52 (1995) 4009–4015.

[37] P.D. Olmsted, C.Y.D. Lu, Coexistence and phase separation in sheared complex fluids, Phys. Rev. E 56 (1997) 55–58.

[38] E.K. Wheeler, P. Fischer, G.G. Fuller, Time-periodic flow induced structures and instabilities in a viscoelastic surfactant solution, J. Non-Newtonian Fluid Mech. 75 (1998) 193–208.

[39] J.Y. Lee, G.G. Fuller, N. Hudson, X.-F. Yuan, Investigation of shear-banding structure in wormlike micellar solution by pointwise flow-induced birefringence measurements, J. Rheol. 49 (2005) 537–550.

[40] M.E. Cates, T.C.B. McLeish, G. Marrucci, The rheology of entangled polymers at very high shear rates, Europhys. Lett. 21 (1993) 451–456.

[41] H. Rehage, H. Hoffmann, Viscoelastic surfactant solutions: model systems for rheological research, Mol. Phys. 74 (1991) 933–973.

[42] T. Shikata, H. Hirata, E. Takatori, K. Osaki, Nonlinear viscoelastic behavior of aqueous detergent solutions, J. Non-Newtonian Fluid Mech. 28 (1988) 171–182.

[43] P. Fischer, E.K. Wheeler, G.G. Fuller, Shear-banding structure orientated in the vorticity direction observed for equimolar micellar solution, Rheol. Acta 41 (2002) 35–44.

[44] P. Fischer, Time dependent flow in equimolar micellar solutions: transient behaviour of the shear stress and first normal stress difference in shear induced structures coupled with flow instabilities, Rheol. Acta 39 (2000) 234–240.

[45] S.M. Fielding, P.D. Olmsted, Kinetics of the shear banding instability in startup flows, Phys. Rev. E 68-036313 (2003) 1–20.

[46] A. Aradian, M.E. Cates, Instability and spatiotemporal rheochaos in a shear-thickening fluid model, Europhys. Lett. 70 (2005) 397–403.

[47] L. Bécu, S. Manneville, A. Colin, Spatiotemporal dynamics of wormlike micelles under shear, Phys. Rev. Lett. 93 (2004) 1–4.

[48] S. Manneville, J.B. Salmon, A. Colin, A spatio-temporal study of rheo-oscillations in a sheared lamellar phase using ultrasound, Eur. Phys. J. E: Soft Matter 13 (2004) 197–212.

[49] G. Porte, J.F. Berret, J.L. Harden, Inhomogeneous flows of complex fluids: mechanical instability versus non-equilibrium phase transition, J. Phys. II 7 (1997) 459–472.

[50] H. Tanaka, Inhomogeneous flow in a one-component polymeric fluid with a nonmonotonic constitutive law, J. Phys. Soc. Jpn. 69 (2000) 299–302.

[51] N.Z. Handzy, A. Belmonte, Oscillatory rise of bubbles in wormlike micellar fluids with different microstructures, Phys. Rev. Lett. 92-124501 (2004) 1–4.

[52] A. Jayaraman, A. Belmonte, Oscillations of a solid sphere falling through a wormlike micellar fluid, Phys. Rev. E 67-065301 (2003) 1–4.

[53] S. Chen, J.P. Rothstein, Flow of a wormlike micelle solution past a falling sphere, J. Non-Newtonian Fluid Mech. 116 (2004) 205–234.

[54] L.B. Smolka, A. Belmonte, Drop pinch-off and filament dynamics of wormlike micellar fluids, J. Non-Newtonian Fluid Mech. 115 (2003) 1–25.

[55] M.C. Sostarecz, A. Belmonte, Beads-on-string phenomena in wormlike micellar fluids, Phys. Fluids 16 (2004) L67–L70.

[56] R.K. Prudhomme, G.G. Warr, Elongational flow of solutions of rodlike micelles, Langmuir 10 (1994) 3419–3426.

[57] L.M. Walker, P. Moldenaers, J.F. Berret, Macroscopic response of wormlike micelles to elongational flow, Langmuir 12 (1996) 6309–6314.

[58] P. Fischer, G.G. Fuller, Z.C. Lin, Branched viscoelastic surfactant solutions and their response to elongational flow, Rheol. Acta 36 (1997) 632–638.

[59] B. Lu, X. Li, L.E. Scriven, H.T. Davis, Y. Talmon, J.L. Zakin, Effect of chemical structure on viscoelasticity and extensional viscosity of drag-reducing cationic surfactant solutions, Langmuir 14 (1998) 8–16.

[60] C.M. Chen, G.G. Warr, Light scattering from wormlike micelles in an elongational field, Langmuir 13 (1997) 1374–1376.

[61] P. Dontula, M. Pasquali, L.E. Scriven, C.W. Macosko, Can extensional viscosity be measured with opposed nozzle devices? Rheol. Acta 36 (1997) 429–448.

[62] M. Kato, T. Takahashi, M. Shirakashi, Steady planar elongational viscosity of CTAB/NaSal aqueous solutions measured in a 4-roll mill flow cell, J. Soc. Rheol. Jpn. 30 (2002) 283–287.

[63] A.J. Muller, M.F. Torres, A.E. Saez, Effect of the flow field on the rheological behavior of aqueous cetyltrimethylammonium p-toluenesulfonate solutions, Langmuir 20 (2004) 3838–3841.

[64] V.J. Anderson, P.M.J. Tardy, J.P. Crawshaw, G.C. Maitland, Extensional flow of micellar fluids, in: Proceedings of the XIVth International Congress on Rheology, Seoul, Korean Society of Rheology, FE03, 2004, pp. 1–3.

[65] J.P. Rothstein, Transient extensional rheology of wormlike micelle solutions, J. Rheol. 47 (2003) 1227–1247.

[66] S.L. Anna, G.H. McKinley, Elasto-capillary thinning and breakup of model elastic liquids, J. Rheol. 45 (2001) 115–138.

[67] V.M. Entov, E.J. Hinch, Effect of a spectrum of relaxation times on the capillary thinning of a filament of elastic liquid, J. Non-Newtonian Fluid Mech. 72 (1997) 31–53.

[68] M. Stelter, G. Brenn, A.L. Yarin, R.P. Singh, F. Durst, Validation and application of a novel elongational device for polymer solutions, J. Rheol. 44 (2000) 595–616.

[69] M.E. Cates, S.J. Candau, Statics and dynamics of worm-like surfactant micelles, J. Phys. Condens. Matter 2 (1990) 6869–6892.

[70] M. Doi, S.F. Edwards, The Theory of Polymer Dynamics, Clarendon Press, Tokyo; Cambridge, 1989.

[71] S.J. Candana, E. Hirsch, R. Zana, M. Adam, Network properties of semidilute aqueous KBr solutions of cetyltrimethylammonium chloride, J. Colloid Interface Sci. 122 (1989) 430–440.

[72] S.A. Safran, P.A. Pincus, M.E. Cates, F.C. Macintosh, Growth of charged micelles, J. Phys. 51 (1990) 503–510.

[73] S.J. Candau, A. Khatory, F. Lequeux, F. Kern, Rheological behavior of wormlike micelles—effect of salt content, J. Phys. IV 3 (1993) 197–209.

[74] T. Shikata, T. Kotaka, Entanglement network of thread-like micelles of a cationic detergent, J. Non-Cryst. Solids 131 (1991) 831–835.

[75] T.M. Clausen, P.K. Vinson, J.R. Minter, H.T. Davis, Y. Talmon, W.G. Miller, Viscoelastic micellar solutions—microscopy and rheology, J. Phys. Chem. 96 (1992) 474–484.

[76] F. Kern, P. Lemarechal, S.J. Candau, M.E. Cates, Rheological properties of semidilute and concentrated aqueous-solutions of cetyltrimethylammonium bromide in the presence of potassium-bromide, Langmuir 8 (1992) 437–440.

[77] H.A. Barnes, A review of the slip (wall depletion) of polymer solutions, emulsions and particle suspensions in viscometers: Its cause, character, and cure, J. Non-Newtonian Fluid Mech. 56 (1995) 221–251.

[78] C. Grand, J. Arrault, M.E. Cates, Slow transients and metastability in wormlike micelle rheology, J. Phys. II 7 (1997) 1071–1086.

[79] M.M. Britton, P.T. Callaghan, Nuclear magnetic resonance visualization of anomalous flow in cone-and-plate rheometry, J. Rheol. 41 (1997) 1365–1386.

[80] M.M. Britton, P.T. Callaghan, Shear banding instability in wormlike micellar solutions, Eur. Phys. J. B 7 (1999) 237–249.

[81] E. Cappelaere, J.F. Berret, J.P. Decruppe, R. Cressely, P. Lindner, Rheology, birefringence, and small-angle neutron scattering in a charged micellar system: evidence of a shear-induced phase transition, Phys. Rev. E 56 (1997) 1869–1878.

[82] J.F. Berret, R. Gamez-Corrales, Y. Serero, F. Molino, P. Lindner, Shear-induced micellar growth in dilute surfactant solutions, Europhys. Lett. 54 (2001) 605–611.

[83] J.P. Decruppe, S. Lerouge, J.F. Berret, Insight in shear banding under transient flow, Phys. Rev. E 63-022501 (2001) 1–4.

[84] Y.T. Hu, P. Boltenhagen, D.J. Pine, Shear thickening in low-concentration solutions of wormlike micelles: I. Direct visualization of transient behavior and phase transitions, J. Rheol. 42 (1998) 1185–1208.

[85] J.F. Le Meins, J.F. Tassin, Shear-induced phase separation in an associating polymer solution, Macromolecules 34 (2001) 2641–2647.

[86] J.F. Berret, R. Gamez-Corrales, S. Lerouge, J.P. Decruppe, Shear-thickening transition in surfactant solutions: new experimental features from rheology and flow birefringence, Eur. Phys. J. E 2 (2000) 343–350.

[87] J.P. Decruppe, R. Cressely, R. Makhloufi, E. Cappelaere, Flow birefringence experiments showing a shear-banding structure in a CTAB solution, Colloid Polym. Sci. 273 (1995) 346–351.

[88] S. Lerouge, J.P. Decruppe, J.F. Berret, Correlations between rheological and optical properties of a micellar solution under shear banding flow, Langmuir 16 (2000) 6464–6474.

[89] F.E. Caputo, V.M. Ugaz, W.R. Burghardt, J.F. Berret, Transient 1–2 plane small-angle X-ray scattering measurements of micellar orientation in aligning and tumbling nematic surfactant solutions, J. Rheol. 46 (2002) 927–946.

[90] O. Radulescu, P.D. Olmsted, J.P. Decruppe, S. Lerouge, J.F. Berret, G. Porte, Time scales in shear banding of wormlike micelles, Europhys. Lett. 62 (2003) 230–236.

[91] M.W. Johnson, D. Segalman, Model for viscoelastic fluid behavior which allows non-affine deformation, J. Non-Newtonian Fluid Mech. 2 (1977) 255–270.

[92] F. Greco, R.C. Ball, Shear-band formation in a non-Newtonian fluid model with a constitutive instability, J. Non-Newtonian Fluid Mech. 69 (1997) 195–206.

[93] C.Y.D. Lu, P.D. Olmsted, R.C. Ball, Effects of nonlocal stress on the determination of shear banding flow, Phys. Rev. Lett. 84 (2000) 642–645.

[94] N. Phan-Thien, R.I. Tanner, New constitutive equation derived from network theory, J. Non-Newtonian Fluid Mech. 2 (1977) 353–365.

[95] J.L. White, A.B. Metzner, Development of constitutive equations for polymeric melts and solutions, J. Appl. Polym. Sci. 7 (1963) 1869–1891.

[96] R.B. Bird, J.R. deAguiar, An encapsulated dumbbell model for concentrated polymer-solutions and melts. 1. Theoretical development and constitutive equation, J. Non-Newtonian Fluid Mech. 13 (1983) 149–160.

[97] R.G. Larson, Constitutive Equations for Polymer Melts and Solutions, Butterworth-Heinemann, New York, 1988.

[98] B. Yesilata, A. Öztekin, S. Neti, Non-isothermal viscoelastic flow through an axisymmetric sudden contraction, J. Non-Newtonian Fluid Mech. 89 (2000) 133–164.

[99] J.P. Rothstein, G.H. McKinley, Nonisothermal modifications of purely elastic instabilities in torsional flows of polymeric fluids, Phys Fluids 13 (2001) 382–396.

[100] B. Yesilata, A. Öztekin, S. Neti, Instabilities in viscoelastic flow through an axisymmetric sudden contraction, J. Non-Newtonian Fluid Mech. 87 (1999) 35–62.

[101] G.H. McKinley, P. Pakdel, A. Öztekin, Rheological and geometric scaling of purely elastic flow instabilities, J. Non-Newtonian Fluid Mech. 67 (1996) 19–47.